THESIS

PARAMETER ESTIMATION METHODS FOR MODELS OF MAJOR FLOOD EVENTS IN UNGAUGED MOUNTAIN BASINS OF COLORADO

Submitted by

Ben Christopher Irvin IV

Department of Civil and Environmental Engineering

In partial fulfillment of the requirements

For the Degree of Master of Science

Colorado State University

Fort Collins, Colorado

Fall 2021

Master's Committee:

Advisor: Jeffrey D. Niemann

Russ S. Schumacher
Ryan Bailey

ABSTRACT

PARAMETER ESTIMATION METHODS FOR MODELS OF MAJOR FLOOD EVENTS IN UNGAUGED MOUNTAIN BASINS OF COLORADO

Accurate hydrologic modeling of ungauged mountain basins plays an important role in ensuring the safety of Colorado's dams. Recent research has shown that infiltration-excess runoff, saturation-excess runoff, and subsurface stormflow can all contribute to streamflow from major storms in Colorado's mountains, and the soil moisture accounting (SMA) method in HEC-HMS has been suggested as an appropriate approach to model these mechanisms. However, SMA requires estimation of parameters that have not been previously considered in dam safety analyses. The objectives of this work are to (1) evaluate simplifications to the modeling process that would reduce the number of required parameters and (2) develop methods to estimate the remaining parameters in ungauged mountain basins of Colorado where calibration to observed discharges is not possible. The proposed simplifications and parameter estimation methods are tested for five basins in the Front Range and three basins in the San Juan Range that have streamflow data available for major flood events. For these historical events, the proposed uncalibrated models produce the same streamflow generation processes as calibrated models and the predicted peak discharges from the uncalibrated models usually have 25% errors or smaller. For design storms, the peak discharges from the proposed uncalibrated models can differ substantially from the peak discharges from calibrated models but are conservative relative to the envelope of observed peak discharges.

ACKNOWLEDGMENTS

I would first like to thank my thesis advisor Dr. Jeffrey Niemann for his assistance and guidance during this project. His ability to teach and motivate me to produce my best possible work has been invaluable during my time at Colorado State University, and I am truly grateful. I would also like to thank Mark Perry, Kallie Bauer, and Bill McCormick, of Colorado Dam Safety for their continuous input and support. Not every graduate student gets the opportunity to work on such an impactful project alongside great people, and that is not lost on me. I am also appreciative of the Colorado Water Conservation Board, the Federal Emergency Management Agency, and Colorado Dam Safety for financial support as well as Applied Weather Associates for supplying precipitation data. My thesis would not have been possible if not for them. I would like to acknowledge Bob Jarrett for his input to this study. His expertise proved extremely helpful. I would also like to acknowledge Ryan Bailey and Russ Schumacher for participating on my master's committee and providing a valuable outside perspective. Finally, I am grateful for my family, especially my mom, Sheryl. Her emphasis on the value of education and unwavering support inspired my ambition to move to Colorado to pursue a master's degree.

TABLE OF CONTENTS

LIST OF TABLES

LIST OF FIGURES

1. INTRODUCTION

The Dam Safety Branch of Colorado's Division of Water Resources (DWR) is responsible for ensuring the safety of approximately 2,000 dams throughout Colorado. Hydrologic models play an important role in the design and evaluation of safety of these dams. Typically, design storms are first generated based on the Colorado and New Mexico Regional Extreme Precipitation Study (REPS) (DWR and New Mexico Office of the State Engineer, 2018). These design storms include the probable maximum precipitation (PMP) and annual exceedance probability (AEP) events. Then, hydrologic models are used to estimate the streamflow that is generated from the design storms. The predicted peak flows and volumes at the dam location are used to determine spillway sizing and freeboard requirements.

Colorado's current guidelines assume that streamflow is generated by infiltration-excess runoff and recommend modeling runoff production using the Green and Ampt method (Sabol, 2008) or the initial and constant loss method (FERC, 2001). Infiltration-excess runoff occurs when the rainfall intensity exceeds a nonzero infiltration capacity of the soil (Horton, 1940). However, through an examination of several historical floods in Colorado's Front Range, Woolridge et al. (2020) found that infiltration-excess runoff, saturation-excess runoff, and subsurface stormflow can all contribute to streamflow. Saturation-excess runoff occurs when rain falls on soil that is completely saturated from a layer of low permeability up to the soil surface (Dunne and Black, 1970a; Dunne and Black, 1970b). Subsurface stormflow is the downslope movement of infiltrated water on a low permeability layer (Kirkby and Chorley, 1967).

Woolridge et al. (2020) used the soil moisture accounting (SMA) loss method within Hydrologic Engineering Center - Hydrologic Modeling System (HEC-HMS) (Bennett et al., 1998; Bennett et al., 2000) to simulate the three observed streamflow production mechanisms.

They disaggregated the study basins into sub-basins in order to better represent the spatial variation of precipitation. They further divided the sub-basins into north-facing and south-facing components to account for aspect-related differences in vegetation and soil. The Clark method was used to transform runoff into streamflow, and a linear reservoir was used to transform subsurface stormflow into streamflow. This modeling approach reproduces the active streamflow mechanisms for the observed floods in the Front Range, but several parameters were estimated by calibrating to streamflow observations (Woolridge et al., 2020). Calibration is not possible in many pratical dam safety applications because most Colorado dams are in ungauged basins. Furthermore, no guidance is available in the scientific literature regarding SMA model parameter estimation, although several studies have provided or recommend calibrated parameter values (Sorooshian et al., 1993; Bennett et al., 2000; Feldman, 2000).

In the literature, three general approaches have been proposed to predict streamflow in ungauged basins. The first method is regionalization, which transfers calibrated parameter values from one or more gauged basins to the ungauged basin (Bloschl and Sivapalan, 1995). The gauged basins can be selected based on their proximity or similarity to the ungauged basin, and the choice of the gauged basins impacts the model performance in the ungauged basin (Zhang and Chiew, 2009). The second method is regression, which uses gauged basins to establish empirical relationships between the parameter values and basin attributes. The basin attributes need to characterize the factors that determine the hydrological response and must be derivable from available data (Kokkonen et al., 2003). Such attributes can include geomorphic, soil, vegetation, and geological properties, which can be obtained from digital elevation models (DEMs), landcover data, and soil maps, respectively. Once the relationships are established, the parameter values for the ungauged basin are estimated from the relationships and the basin's attributes (Zhang and Chiew, 2009). The third approach is ensemble modeling or model averaging (McIntyre et al., 2005). In this approach, the results of different models of gauged basins are averaged to provide an estimate of streamflow in the ungauged basin. This approach produces a range of possible streamflow estimates, which can provide an indication of the uncertainty in the estimated flow (McIntyre et al., 2005).

The preferred method for prediction in ungauged basins remains unclear. Zhang and Chiew (2009) found that a regionalization approach that combines spatial proximity and physical similarity outperforms regionalization based on spatial proximity or physical similarity alone. Samuel et al. (2011) also found that a coupled similarity-proximity approach leads to the better performance. Razavi and Coulibaly (2013) examined whether different methods perform better in different regions or climates. They found that transferring parameters based on proximity and similarity works best in arid to temperate climates as well as cold and snowy regions. In contrast, regression-based methods appear to work best in warm temperate regions. McIntyre et al. (2005) found that ensemble modeling and model averaging perform better than the regression-based approach.

All these studies considered large numbers of gauged basins and storm events to predict streamflow in ungauged basins. Zhang and Chiew (2009) considered 210 basins in southeast Australia. Samuel et al. (2011) considered 94 basins in Ontario, Canada. McIntyre et al. (2005) considered 127 basins in the United Kingdom. In Colorado’s mountains, well-documented flood events are extremely rare (Colorado Division of Water Resources and New Mexico Office of the State Engineer, 2018), which limits the applicability of sophisticated approaches.

Several studies have also found benefits from reducing the number of parameters that must be estimated. For example, Caldwell et al. (2015) found that simpler models have comparable performance to more complex, fine-scale models. A more lumped approach to hydrologic modeling can increase overall model accuracy by reducing errors from uncertain parameters (Reed et al., 2004). Additionally, models with more parameters are more prone to equifinality, where many different parameter sets can produce the same model outcome (Beven, 1993). Kampf and Burges (2007) suggest representing the dominant flow processes while minimizing the number of uncertain parameters.

The objectives of this research are to (1) evaluate simplifications to the SMA modeling approach of Woolridge et al. (2020) that would reduce the number of required parameters and (2) develop methods to estimate the remaining parameters in ungauged mountain basins of Colorado. The proposed parameter estimation method is similar to the regression approach because relationships are established between the parameter values and watershed characteristics in gauged basins and those relationships are assumed to apply in ungauged basins. However, because only a few extreme storm events have adequate data in the Colorado mountains, the relationships are developed based on the literature and assumptions rather than regression techniques. We refer to the resulting models as uncalibrated because the parameters are not adjusted in individual basins to match the streamflow observations. The uncalibrated modeling approach is developed and evaluated using five basins in the Front Range and three basins in the San Juan Range. The modeling approach is first evaluated by simulating historical floods and comparing to observed flows and the results of calibrated models. The historical events are also used to examine the errors that are introduced by individual parameter estimation methods. Then, the uncalibrated models are evaluated by simulating the discharge from AEP and PMP design storms and comparing to the results of calibrated models and other independent estimates of extreme flows.

The outline for this study is as follows. Chapter 2 discusses the study basins, historical storms, and design storms that are considered. Chapter 3 details the modeling methods including the proposed model simplifications and parameter estimation techniques. Chapter 4 presents the model results for the historical storms and design storms. Chapter 5 discusses the implications of the model results, and Section 6 provides the main conclusions of the study.

2. STUDY BASINS AND EVENTS

2.1 Basins

Eight basins were selected for modeling because they have experienced significant floods for which precipitation and streamflow data are available. Five of the basins are in the Front Range, and three are in the San Juan Range (Fig. 1). Basic characteristics of the basins can be found in Table 1. Mineral Creek and Vallecito Creek are in the heart of the San Juan Range, while Saguache Creek is in the Cochetopa Hills, which connect the San Juan and Sawatch ranges.

The Front Range is in north-central Colorado. It is a Laramide range with a core of Precambrian crystalline rock (gneiss and granodiorite) and uplifted adjacent Mesozoic sedimentary rock (Dickinson et al., 1988; Anderson et al., 2015). Common vegetation types include lodgepole pine, aspen, Douglas fir, limber pine, shrubs, and herbaceous understory (Anderson et al., 2001; Ebel, 2013). At low elevations, the north-facing slopes are primarily forested while south-facing slopes are shrublands (Ebel, 2013). At intermediate elevations, hillslopes are primarily forested irrespective of their aspect. High elevations are above timberline and have sparse vegetation with abundant rock outcrops and small alpine lakes. Soils typically have high sand content (gNATSGO, 2020).

The San Juan Range is in southwestern Colorado. It is geologically complex with a core of Precambrian crystalline rocks, localized areas of volcanism and intrusive igneous rock, and sedimentary rocks along the range margins (Chimner et al., 2009). Ash-flow tuffs and Basalt flows and associated tuff and breccia are also present (Tweto and Ogden, 1979). Common vegetation types include ponderosa pine, Mexican white pine, subalpine fir, Colorado blue spruce, shrubby cinquefoil, and rabbitbrush (Zier and Baker, 2006). Like the Front Range, the high elevations are above timberline with abundant rock outcrops and small alpine lakes. Soils have lower sand content than the Front Range (gNATSGO, 2020).

2.2 Historical Storms

A summary of the historical storms and corresponding basins is provided in Table 2. All four flood-generating storm types in REPS (DWR and New Mexico Office of the State Engineer 2018) are included in the dataset. A mesoscale storm with embedded convection (MEC) occurred over the North Fork of the Big Thompson River basin in 1976 (McCain et al., 1979). Mid-latitude cyclone (MLC) events occurred over Cheyenne Creek in 1997 and over most of the Front Range in 2013 (Gochis et al., 2013). Another MLC event occurred over Mineral Creek and Vallecito Creek in 2006 (FEMA, 2010). A tropical storm remnant (TSR) event occurred over Vallecito Creek in 1970 (Roeske, 1971), and another TSR occurred over Mineral Creek and Vallecito Creek in 2004. A local storm (LS) event occurred over the northeast portion of the Saguache Creek basin in 1999 (Cotton et al., 2003).

Rainfall data for the historical storms were obtained from Storm Precipitation Analysis System (SPAS) (Parzybok and Tomlins, 2006). SPAS uses rain gauge and radar data to estimate the spatial (36 arc-second resolution) and temporal (1 hour resolution) patterns of precipitation (MetStat, 2018). NEXRAD radar (Heiss et al., 1990) became available in the mid-1990s, so precipitation estimates after this date are expected to be more accurate. Vertical polarization of the signal began in 2006, which helps identify hail contamination and further improves the estimates (Hubbert and Pratte, 2006). A NEXRAD radar is available in Denver, which is adjacent to the Front Range. At the time of the historical storms, the nearest NEXRAD radars to the San Juan range were in Grand Junction and Pueblo. Because these radars are far from the range (~150 km), the beam is high and diffusive, which leads to lower accuracy in the precipitation rates for San Juan storms (Kitchen and Jackson, 1993; Smith et al., 1996; Young et al., 1999).

Streamflow data were obtained from Colorado Division of Water Resources gauges, which typically have a 15-minute resolution. However, for the Vallecito Creek 1970 event, only daily average flows and the peak flow are available. For the North Fork Big Thompson River 1976 event, only a partial hydrograph is available, but it captures the peak flow (McCain et al., 1979). For the Vallecito Creek 2004 event, only a partial hydrograph is available, and it is not known whether the peak flow was captured. The Front Range storms usually produced higher ratios between the observed peak flows and the StreamStats 100-yr flows (Capesius and Stephens, 2009) than the San Juan Range storms (Table 2). The North Fork Big Thompson River 1976 event produced the highest ratio among all the events.

The highest runoff coefficients occurred in Mineral Creek and Vallecito Creek for the 2006 storm (Table 2). A flood insurance study by FEMA (2010) suggested that rain-on-snow occurred for event, which could explain the high runoff coefficients. However, an examination of nearby Snow Telemetry (SNOTEL) sites did not show a clear melting of snowpack. Saguache Creek 1999 has a much lower runoff coefficient than the other basins/storms. The lower value occurs in part because the 1999 storm only occurred in a part of this large basin. If the runoff coefficient is calculated using the storm area rather than the basin area, it increases to 0.09 but remains below the other values in Table 2. The Saguache Creek 1999 runoff coefficient is discussed in greater detail later in the paper.

2.3 Design Storms

The design storms were obtained from REPS. 2-hr LS events, 6-hr MEC events, and 48-hr MLC events with AEPs between 10^{-1} to 10^{-7} are modeled in each basin. Three PMP storms (2-hr, 6-hr, and 72-hr) are also modeled in each basin. In REPS, the AEP rainfall estimates are produced using a 4-parameter kappa distribution that does not have an upper bound, which allows the AEP frequency curve to cross the PMP on occasion (DWR and New Mexico Office of the State Engineer, 2018). Thus, it is possible for a very rare AEP storm to exceed the PMP.

3. PARAMETER ESTIMATION METHODOLOGY

3.1 Model Components

The main components and processes included in each sub-basin of the HEC-HMS models are presented in Fig. 2. The components and processes are the same as in Woolridge et al. (2020). Rainfall first enters the canopy storage, which represents the interception of rainfall by vegetation. This storage must be filled before precipitated water can enter other storage volumes (Feldman, 2000). Water in the canopy storage is held until it is removed by evapotranspiration (ET). Surface storage (i.e. depression storage) is not explicitly represented in the models. Because the canopy and surfaces storages behave the same way if included in SMA, the canopy storage element may implicitly represent some surface storage in the models.

When canopy storage is overcome, rainfall becomes throughfall and can contribute to the soil storage. The infiltration capacity of the soil depends in part on the current soil storage. The soil storage includes water that attaches to the soil particles and can only be removed by ET (i.e. tension storage). It also includes water that fills the pore spaces between the soil particles and can be removed by ET or gravity drainage (i.e., gravity storage) (Feldman, 2000). Excess rainfall is transformed into streamflow at the sub-basin outlet by the Clark (1945) method. This method uses a dimensionless time-area curve and the time of concentration to account for the translation of flow to the sub-basin outlet. It also uses a linear reservoir to account for sub-basin storage effects (Clark 1945).

When the soil storage exceeds the maximum tension storage, water can enter groundwater storage via soil percolation. The groundwater layer represents any saturated layer on top of the bedrock or other restrictive layer (Feldman, 2000). Outflow from this layer depends in part on its current storage. The outflow is converted into streamflow at the sub-basin outlet by a linear reservoir. The outflow from the linear reservoir is a function of the current reservoir storage and a specified time constant.

River routing describes the transfer of flow through channels and is needed to combine flows from upper and lower sub-basins. The Muskingum-Cunge method is used for routing because it includes flood-wave advection and attenuation (Feldman, 2000), and it allows overbank flows, which are expected for extreme events (Woolridge et al., 2020).

Reservoir routing describes the effects of storage in a lake behind a dam (Feldman, 2000). Only the South Boulder Creek basin contains a reservoir (Gross Reservoir) and uses reservoir routing. An elevation-storage-discharge relationship, specification of an outlet structure, and initial conditions are used in the reservoir routing. These relationships were obtained for Gross Reservoir from DWR and Denver Water.

Source elements in HEC-HMS describe point inflows to the stream network, and diversion elements describe point outflows from the network (Feldman, 2000). Moffatt Tunnel, which moves water under the continental divide, is modeled as a source in the South Boulder Creek model using specified flows from DWR. The South Boulder Creek diversion is also modeled using specified flows from DWR.

3.2 Basin Disaggregation

HEC-HMS assumes that rainfall and watershed properties are spatially uniform within sub-basins. Woolridge et al. (2020) disaggregated each basin into sub-basins to capture rainfall variations (Zhang et al., 2004) and then into the north-facing and south-facing portions of each sub-basin to capture aspect dependent watershed properties. We use the same sub-basin disaggregation method as Woolridge et al. (2020) while neglecting the separate consideration of north-facing and south-facing hillslopes. The sub-basins were determined using 1/3 arc-second resolution (~10 m) DEM from the USGS National Elevation Dataset (USGS, 2020a). The channel network was developed from the DEM using a contributing area threshold, and a sub-basin was included for each source and link in the channel network (Djokic et al., 2011). A 15 km^2 threshold is used because the resulting sub-basins have relatively uniform rainfall in space while the number of sub-basins remains low (Woolridge et al., 2020). A step-by-step procedure for model creation and sub-basin disaggregation is provided in Appendix A. The sub-basins for the Big Thompson River basin are also shown in Appendix C.

3.3 Data Sources for Parameter Estimation

An overview of the proposed parameter estimation procedure is provided in Fig. 3. The parameters are estimated from five data sources, which are available for ungauged watersheds in Colorado. Landsat 8 imagery (USGS, 2020b) is used to characterize the vegetation density and its effect on soil hydraulic properties. From Landsat 8, we use the Normalized Difference Vegetation Index (NDVI), which is a measure of surface greenness (Montandon and Small, 2008). Fractional vegetation cover is then computed from NDVI using a linear function (Montandon and Small, 2008; Vermote et al., 2016). The endpoints of the linear function are the NDVI for well-vegetated areas ($NDVI_\infty$) and the NDVI for barren areas ($NDVI_0$). Timilsina et al. (2021) estimated $NDVI_\infty$ to be 0.70 and $NDVI_0$ to be 0.04 for the Front Range. These values are used to estimate fractional vegetation cover in both the Front Range and in the San Juan Range.

Soil parameters are mainly estimated from the NRCS gridded National Soil Survey Geographic database (gNATSGO). gNATSGO relies mainly on the NRCS Soil Survey Geographic Database (SSURGO) but fills gaps in SSURGO's coverage with State Soil Geographic Database (STATSGO2) and Raster Soil Survey Databases (RSS) (gNATSGO, 2020). From gNATSGO, we use percent sand, percent clay, and percent organic matter from the soil surface to a depth of 60 cm. The 60 cm value was chosen based on typical soil depths in the Colorado mountains (gNATSGO, 2020). The depth to any restrictive layer Z_{Soil} is also obtained from gNATSGO. For conservatism and consistency with the soil texture estimates, if the sub-basin average depth to restrictive layer exceeds 60 cm, it is set to 60 cm.

Basic soil hydraulic properties are calculated from the soil texture information using pedotransfer functions (Rawls et al., 1983; Saxton and Rawls, 2006). The outputs of these pedotransfer functions are grids of soil moisture content at saturation θ_s, field capacity θ_{fld}, wilting point θ_{wp}, wetting front suction head ψ_f, and the saturated hydraulic conductivity. The saturated hydraulic conductivity is then adjusted based on the fractional vegetation cover as recommended by Sabol (2008) and divided by two to account for possible unsaturated flow (Woolridge et al., 2020; Bouwer, 1964) to produce the final saturated hydraulic conductivity K_{sat}. The gridded soil hydraulic properties are then averaged to obtain values for each sub-basin. More details on the pedotransfer functions can be found in Appendix B.

Elevation data from the USGS National Elevation Dataset are used in the HEC-HMS terrain processing functions to characterize sub-basin and reach geomorphology. The outputs of this processing include the sub-basin area A, the flow length between the hydraulically most distant point and the outlet L, the watercourse slope S, and the flow length between a point on L that is perpendicular to the watershed centroid and the outlet L_{ca} (Sabol, 2008).

Google Earth satellite imagery (Google, 2020) is used to identify floodplain and channel characteristics. Finally, StreamStats (Capesius and Stephens, 2009) is used to estimate the 2-year flow in each reach of the models. The methods we propose to estimate the parameters from these datasets are described in depth in the following sub-sections. The average parameter values for each basin are provided in Appendix C.

3.4 Canopy Parameters

The canopy model requires estimation of three parameters: maximum canopy storage, initial canopy storage, and canopy ET rate. Woolridge et al. (2020) estimated the maximum canopy storage and canopy ET rate using measurements from the Cache la Poudre experimental catchment in the northern Front Range (Traff et al., 2015). In this catchment, throughfall was measured under the dominant vegetation species on north-facing slopes (ponderosa pines) and south-facing slopes (antelope bitterbrush) and rainfall was measured in an open area. Woolridge et al. (2020) calibrated the maximum canopy storage and canopy ET rate for each hillslope orientation to reproduce the observed throughfall rates as closely as possible. We propose using a simple average of the north-facing and south-facing maximum canopy storage values for ungauged basins (4.3 mm). In reality, the canopy storage is expected to vary with the dominant vegetation species and density of vegetation cover (Sabol, 2008), but the quantitative dependence of canopy storage on these factors is poorly understood. Like Woolridge et al. (2020), we assume that the initial canopy storage is zero. Timilsina et al. (2021) determined a function that estimates average daily potential ET as a function of elevation in the Front Range. For ungauged basins, we propose estimating the canopy ET as the average daily potential ET at the average elevation of each sub-basin. This procedure assumes that the canopy ET occurs at the potential ET rate and that the dependence of potential ET on elevation observed in the Front Range applies to other ranges in Colorado.

3.5 Soil Layer Parameters

The soil layer model requires specification of six parameters: maximum infiltration rate, maximum soil storage, tension storage, initial soil storage, soil percolation rate, and imperviousness. The maximum infiltration rate f is the highest rate at which water can enter the soil layer. Following Woolridge et al. (2020), we propose estimating f as the Green and Ampt (1911) infiltration rate when the wetting front is near the ground surface:

$$f = K_{sat}\left[1 + \frac{|\psi_f|}{\delta}\right] \quad (1)$$

In this expression, δ is the depth of the wetting front, which is selected as 75 mm following Woolridge et al. (2020) and Sabol (2008).

Maximum soil storage S_{max} represents the total water that can be stored and removed from the soil layer including both tension and gravity storage. For ungauged basins, we propose estimating S_{max} based on an approach Koren et al. (2000) suggested for the Sacramento Soil Moisture Accounting Model (SAC-SMA) (Burnash et al. 1995). Specifically:

$$S_{max} = (1 - P_{GW})Z_{Soil}(\theta_{sat} - \theta_{wp}) \quad (2)$$

where P_{GW} is the fraction of the soil column above the restrictive layer that is dedicated to groundwater storage. The wilting point is subtracted in Eq. 2 because no natural mechanism can lower the soil moisture below the wilting point. P_{GW} is difficult to estimate because the thickness of the groundwater layer likely varies between events. $P_{GW} = 0.10$ was selected based on model performance.

We propose estimating tension storage S_{ten} also following Koren et al. (2000). Specifically:

$$S_{ten} = (1 - P_{GW})Z_{Soil}(\theta_{fld} - \theta_{wp}) \quad (3)$$

In SMA, the groundwater layer does not consider tension storage (Bennet et al., 1998; Feldman, 2000), so any water stored in the groundwater layer can drain. However, the groundwater layer represents the bottom of the soil column, so tension storage is expected to occur in reality. Because such storage cannot be included in the groundwater layer, it is included in the soil layer by increasing θ_{fld} by 30%.

The soil percolation rate is the maximum rate at which water leaves the soil layer and enters the groundwater layer. We assume that the soil percolation occurs as gravity drainage (i.e. without a gradient in soil suction). In that case, Darcy's Law indicates that the percolation rate is K_{sat}. We propose using K_{sat} as the soil percolation rate in ungauged basins.

The initial soil storage is the portion of the maximum soil storage that is occupied by water at the start of the simulation. For the historical storms, this value is estimated from nearby soil moisture sensors if available and otherwise calibrated. For the 2013 storm in the Front Range, the initial soil storage was estimated from the soil moisture sensors at the National Science Foundation's Boulder Creek Critical Zone Observatory (Anderson et al., 2019). Sensor depths ranged from 5 cm to 138 cm. For the 2004 and 2006 storms in the San Juan Range, soil moisture data were obtained from Snow Telemetry (SNOTEL) stations. Sensors are available at depths of 5 cm, 10 cm, and 50 cm. For all other historical storms, the initial soil moisture was determined through calibration. For the design storms and ungauged basins, we propose estimating the initial soil moisture as the adjusted field capacity (Sabol, 2008).

The imperviousness is defined as the portion of a sub-basin for which all precipitation becomes runoff (Feldman, 2000). Natural imperviousness can occur in mountain basins as bedrock outcrops and canyon walls, but it is difficult to quantify. Landcover datasets are known to underestimate natural imperviousness by large margins (Petliak et al., 2019). Woolridge et al. (2020) neglected imperviousness. We evaluated estimating natural imperviousness as the portion of the sub-basin where the depth to any soil restrictive layer is zero (gNATSGO, 2020). We also considered treating any soil units with a leading descriptor of "bedrock" as impervious. However, these approaches are speculative, particularly because they do not consider the hydrologic connectivity of the imperviousness. Other mountain hydrology studies have used values between 2% and 5% for imperviousness (Ahl et al., 2008; Din et al., 2019). Consequently, 5% imperviousness is proposed for ungauged basins in Colorado.

3.6 Transform Parameters

The Clark transform method requires specification of a dimensionless time-area curve that describes the cumulative distribution of travel times from each point to the sub-basin outlet (Clark, 1945; Feldman, 2000). Woolridge et al. (2020) obtained a time-area distribution for each sub-basin using cumulative travel time rasters generated from the DEM, landcover data, and an approximation of Manning's equation. We propose using the default dimensionless time-area curve in HEC-HMS, which is:

$$A_t/A = \begin{cases} 1.414(t/T_c)^{1.5} & t \leq T_c/2 \\ 1 - 1.414(1 - t/T_c)^{1.5} & t > T_c/2 \end{cases} \quad (4)$$

where T_c is the time of concentration, t is a time between 0 and T_c, and A_t is the area of the sub-basin contributing flow at time t.

The Clark method also requires specification of T_c. Woolridge et al. (2020) estimated T_c from the cumulative sub-basin travel time rasters and then calibrated the values as needed. Many empirical equations are available for estimating T_c (see Almeida et al., 2014). We use the expression recommended by Sabol (2008):

$$T_c = 2.47A^{0.078}L^{0.212}L_{ca}^{0.212}S^{-0.263} \quad (5)$$

where sub-basin area A is in km^2, L is in km, S is in m/km, and L_{ca} is in km. We applied several other methods from Almeida et al. (2014) to Cheyenne Creek and found that they produce similar estimates to the Sabol (2008) expression. The Folmar et al. (2007), Linsley (1992), Yen and Chow (1983), and Kirpich (1940) equations estimate T_c within 10 min (9% difference), 20 min (18% difference), 5 min (4% difference), and 15 min (13% difference) of the Sabol estimate, respectively.

The Clark method also requires the linear reservoir storage coefficient R (Feldman, 2000). The storage coefficient is commonly estimated by defining X as:

$$X \equiv R/(R + T_c) \tag{6}$$

and assuming that X remains constant within a given region (FERC, 2001; Dunn et al., 2001; Wang and Dawdy, 2012; Yoo et al., 2014). This is the same as assuming that:

$$R = Z\, T_c \tag{7}$$

where:

$$Z \equiv X/(1 - X) \tag{8}$$

This approach implies that R increases with increasing sub-basin size, and it is consistent with Clark (1945), who considered the basin storage to occur mainly in the channels. However, Zoch (1937) considered the storage to occur mainly in the hillslopes. In such a case, R would remain essentially constant with increasing sub-basin size. For the steep, shallow streams in Colorado's mountain basins, we hypothesize that most of the basin storage occurs in the hillslopes. Thus, rather than using Eq. 6 or 7, we propose using a fixed value R = 7 h for all basins. This approach is directly evaluated later in this study.

3.7 Groundwater Layer Parameters

The groundwater layer model requires specification of four parameters: maximum groundwater storage, groundwater time constant, linear reservoir time constant, and groundwater percolation rate. Woolridge et al. (2020) estimated the groundwater layer parameters through calibration and used higher groundwater percolation rates on south-facing slopes than north-facing slopes.

Maximum groundwater storage S_{GW} represents the maximum amount of water that can be stored in the groundwater layer. For ungauged basins, we propose estimating S_{GW} based on Koren et al. (2000). Specifically:

$$S_{GW} = P_{GW} Z_{Soil} \left(\theta_{sat} - \theta_{wp}\right) \tag{9}$$

The initial groundwater storage is assumed to be zero, which implies that no large storms occurred immediately before the events of interest.

The groundwater time constant within SMA controls the rate that water is released from the groundwater layer, and the linear reservoir time constant within the baseflow method of HEC-HMS controls the rate that the released water is routed to the sub-basin outlet. For simplicity, we assume both time constants have the same value T_{GW}. Many approaches have been proposed to estimate groundwater time constants. Koren et al. (2000) estimated the time constant based on θ_{sat}, θ_{wp}, and a linearization constant. However, this method neglects topographic properties that are known to be important (Freeze, 1972; Freer et al., 2002; Hallema et al., 2016). Other approaches use theoretical relationships with hillslope length, slope, horizontal saturated hydraulic conductivity, soil porosity, and aquifer depth (Kirkby, 1989; Zecharias and Brutsaert, 1998; Samper et al., 2015) to estimate time constants. Periera et al. (1982) proposed regression equations for estimating groundwater time constants for different seasons in the Swiss Alps based on hydraulic conductivity, average basin slope, channel slope, forest cover, and mean seasonal precipitation. Theoretical expressions are difficult to apply because the aquifer depth is unknown and estimating an appropriate hillslope length is difficult, and a regression equation is unlikely to apply outside of the region for which it was developed.

In HEC-HMS, modeled subsurface stormflow is routed to the outlet of the sub-basin completely as groundwater (Feldman, 2000). In reality, subsurface stormflow is expected to travel a shorter distance before it enters the stream network and travels to the sub-basin outlet as streamflow. This subsurface flow distance is expected to control T_{GW}, and it is likely related to the scale of the hillslopes (Zecharias and Brutsaert, 1998; Samper et al., 2015). We propose using a fixed value T_{GW} = 20 h for ungauged basins. This assumption is directly evaluated later in this study.

The groundwater percolation rate determines the net water loss from the system. Woolridge et al. (2020) determined this value through calibration and used different groundwater percolation rates for north-facing and south-facing hillslopes. The groundwater percolation rate is expected to depend on the bedrock material and its jointing and weathering. For the Front Range, we propose using the average rate determined by Woolridge et al. (2020) (2.5 mm/h). For the San Juan Range, we propose using 0.5 mm/h, which was estimated based on the performance of the models.

3.8 River Routing Parameters

The Muskingum-Cunge river routing method requires estimation of channel length, channel slope, cross-section geometry, channel roughness, floodplain roughness, and index flow (Feldman, 2000). Length and slope can be determined using HEC-HMS. The 8-point cross-section option in HEC-HMS is used to represent the channel and floodplain geometry. The channel part of the cross-section is assumed to be rectangular. The width is estimated from the Google Earth satellite imagery, and the depth is determined from Manning's equation and the 2-yr peak flow from StreamStats (Capesius and Stephens, 2009; Woolridge et al., 2020). The floodplain cross-sections are developed using the DEM and the Interpolate Line function in 3D Analyst of ArcMap. Roughness values are assigned based on bed material and riparian vegetation from satellite photos (Chow, 1959). The index flow was estimated as the 2-yr peak streamflow from StreamStats.

4. RESULTS

4.1 Historical Storms

In this section, the uncalibrated models are evaluated by comparing their results to the streamflow observations and the results from the calibrated models for the historical storms. For the Front Range, the calibrated models are from Woolridge et al. (2020). For the San Juan Range, the calibrated models were developed using the procedures described by Woolridge et al. (2020).

Table 3 indicates the runoff mechanism that occurs in the calibrated and uncalibrated models for each storm. All cases produce subsurface stormflow (not indicated in the table), and most cases produce saturation-excess runoff. Following Woolridge et al. (2020), runoff is considered saturation-excess if the soil layer is at least 85% saturated. Only the North Fork Big Thompson 1976 and Saguache Creek 1999 events produce infiltration-excess runoff. The uncalibrated models almost always produce the runoff by the same mechanism as the calibrated models. The exception is Cheyenne Creek 1997 where the calibrated model does not produce surface runoff while the uncalibrated model produces saturation-excess runoff.

Root mean squared error (RMSE), Nash-Sutcliffe coefficient of efficiency (NSCE), and percent error in volume are also shown in Table 3 for the calibrated and uncalibrated models. Moriasi et al. (2007) specified model performance ratings based on NSCE and the RMSE to observations standard deviation ratio. Focusing only on NSCE, they suggested value between 0.50 and 0.65 is classified as "satisfactory," an NSCE between 0.65 and 0.75 is classified as "good," and an NSCE between 0.75 and 1 is classified as "very good." Overall, the uncalibrated models usually perform slightly worse than the calibrated models. The lower performance is expected because the parameters have not been adjusted in each basin to match the observed streamflow hydrograph. For Cheyenne Creek 1997 and Big Thompson River 2013, the uncalibrated models perform better than the previously calibrated models. However, for Mineral Creek 2004 and especially Saguache Creek 1999, the uncalibrated models perform much worse than the calibrated models. Aside from Saguache Creek 1999, which is considered an outlier and is discussed in detail later, the calibrated models consistently produce NSCE values above 0.65, which is consistent with a "good" classification or better. The uncalibrated models also produce NSCE values above 0.65 with the exceptions of Mineral Creek 2004 and Saguache Creek 1999. Overall, the uncalibrated models tend to underestimate the flow volume in the Front Range and overestimate the flow volume in the San Juan Range. The largest underestimation of volume by the uncalibrated models is 25%.

Table 4 shows performance metrics that pertain to peak. Overall, the uncalibrated models perform worse on average than the calibrated models in terms of peak flow error (m^3/s) but better in terms of percent error in peak flow. For percent error in peak flow, the uncalibrated models perform worst for the North Fork Big Thompson River 1976 and Saguache Creek 1999 events, which are the two infiltration-excess cases. The performance at Saguache Creek 1999 is again an outlier compared to the other events. If Saguache Creek 1999 is excluded, the range of percent errors in peak flow is -14% to 25%. On average, the timing of the peak is estimated very well by the calibrated models and relatively well for most of the uncalibrated models. In South Boulder Creek, the uncalibrated model predicts the peak flow much earlier than the observed peak.

Figure 4 shows the observed, calibrated, and uncalibrated streamflow hydrographs for the Front Range events. Overall, the uncalibrated model hydrographs resemble the calibrated model hydrographs with the uncalibrated models usually overestimating peak flow. For the North Fork Big Thompson River 1976 (Fig. 4a), the uncalibrated model has higher peak flow and longer time to peak due to lower infiltration rates and larger values for R and T_c than the calibrated model. For Cheyenne Creek 1997 (Fig. 4b), the uncalibrated model matches the observed peak flow better than the calibrated model because saturation-excess runoff is produced in the uncalibrated model (due to higher tension storage, which makes saturation easier to achieve later in the storm event). For Bear Creek 2013 (Fig. 4e), the uncalibrated model better reproduces the early part of the observed hydrograph but deviates more during the recessions due to shorter groundwater time constants compared to the calibrated model.

Figure 5 shows the observed, calibrated, and uncalibrated streamflow hydrographs for the San Juan Range events. Like in the Front Range, the uncalibrated model hydrographs resemble the calibrated model hydrographs. For Saguache Creek 1999 (Fig. 5b), the uncalibrated model greatly overestimates the peak flow and the total volume. As noted earlier, this event had an anomalously low runoff coefficient (Table 2). The low runoff coefficient could be a real phenomenon, but it could also suggest that the rainfall was overestimated. At the time of the storm, the nearest NEXRAD radar was in Pueblo, which is over 150 km away. Due to this distance, the radar beam is high and diffuse over the Saguache Creek watershed, which could lead to errors (e.g., virga could be interpreted as rainfall). Also, in 1999, radar did not utilize dual polarization, which means hail contamination was more difficult to identify (Hubbert and Pratte, 2006). Finally, SPAS relies on rain gauge data to help translate reflectivities into rainfall rates (MetStat, 2018). No rain gages were located near the center of the storm, so the rescaling used an unofficial rainfall measurement from an unidentified camper (HDR, 2001). To determine how much the rainfall would need to change for the uncalibrated model to reproduce the observed discharge hydrograph, the rainfall rates were multiplied by 50% and 33% in two separate cases and used in the uncalibrated model. As shown in Fig. 5b, the 50% case still overestimates the flow, while the 33% case underestimates the flow. Thus, major adjustments to the precipitation are needed to match the observed hydrograph. An alternative hypothesis is that the watershed characteristics produced the low runoff coefficient. This hypothesis can be evaluated by examining the calibrated parameters when the full rainfall is used. To achieve agreement with the observations, the maximum infiltration rate was increased by a factor of 6, the groundwater percolation rate was increased from 0.5 mm/h to 3.5 mm/h, the initial soil moisture was set to the wilting point, imperviousness was set to zero, and the Clark storage coefficient was reduced from 7 h to 3.5 h. Thus, major adjustments in the watershed characteristics are needed to reproduce the observed flows.

For Mineral Creek 2004, Vallecito Creek 2004, and Mineral Creek 2006 (Fig. 5c, Fig. 5d, and Fig. 5e), the uncalibrated models produce nearly constant flows during the hydrograph recession. This behavior is caused, in part, by the high initial soil storage that was used. This water percolates and eventually saturates the groundwater layer leading to a constant discharge from that layer. This behavior is more pronounced in the uncalibrated models because they have higher maximum groundwater storage values than the calibrated models.

4.2 Effects of Parameter Estimation Methods

Fig. 6 examines how changing the values for groups of parameters affects the model results for a representative case (Big Thompson River 2013). In these experiments, the calibrated model (Woolridge et al., 2020) is the starting point. The parameter values are then changed to the uncalibrated estimates in groups until the uncalibrated model is obtained. Fig. 6a shows the effect of combining the north-facing and south-facing slopes together in the model. Minor changes occur in the model output when this change is made. Fig. 6b shows the results when the Clark method parameters (dimensionless time-area curve, T_c, and R) are also changed to the uncalibrated estimates. For this basin, these changes produce a sharper peak that overestimates the observed peak discharge. The dimensionless time-area curves developed by Woolridge et al. (2020) are positively skewed with a small portion of many sub-basins having much longer travel times than the other areas. Similarly, the T_c values are large compared to the estimates from the Sabol (2008) equation. Replacing both the skewed dimensionless time-area curve with the symmetrical default curve and the large T_c with the shorter T_c from Sabol (2008) consistently neglects the small areas with long travel times and produces little effect on the results. The differences observed in Fig. 6b are due to differences in the linear reservoir time constant R. Fig. 6c shows the results when the soil layer parameters are also changed. The soil layer parameters have more substantial effects than other changes because the soil layer primarily controls runoff production. Thus, these parameters were often calibrated to reproduce the observed hydrographs. Fig. 6d shows the effects of changing the groundwater layer parameters. The groundwater layer parameters strongly effect the recession limb, which is produced by subsurface stormflow. They also affect the overall flow volume because the deep percolation rate determines the water that is lost from the system.

4.3 Design Storms

Figs. 7 and 8 compare the modeled peak flows for the calibrated and uncalibrated models in the Front Range and San Juan range, respectively. In these comparisons, the results from the calibrated models are viewed as the best available estimates, so the uncalibrated models should reproduce these results as accurately as possible. Typically, the differences between the calibrated and uncalibrated peak flows are larger for the shorter duration storms and for the more extreme design storms (e.g., North Fork Big Thompson River, Big Thompson River, and Cheyenne Creek). For the North Fork Big Thompson River (Fig. 7a), the calibrated model uses much shorter values for T_c and R than the uncalibrated model, which produces higher peak flows when surface runoff occurs (shorter duration storms). For Bear Creek (Fig. 7d), differences in the soil layer parameters, primarily soil storage, produce less surface runoff for the uncalibrated model than the calibrated model for almost all design storms. For South Boulder Creek (Fig. 7c), the 72-hr PMP produces low flows in both models due to the effects of Gross Reservoir. Gross reservoir also captures much of the flow from the 2-hr and 6-hr design storms. For Vallecito Creek (Fig. 8b), the uncalibrated model produces saturation-excess runoff later in the 48-hr design storms, which produces lower peak flows than the calibrated model. For Saguache Creek, the uncalibrated model consistently predicts much higher flows than the calibrated model (Fig. 8c). For several 2-hr and 6-hr design storms, the calibrated model does not predict any flow because the maximum infiltration rates are six times higher than those of the uncalibrated model. This behavior is inconsistent with the other basins and supports the hypothesis that the 1999 rainfall was overestimated.

Even if Saguache Creek is excluded from consideration, the flows from the uncalibrated and calibrated models can exhibit substantial differences for the design storms. Fig. 9 plots the distribution of the percent error in the peak flow from all the design storms and basins. A positive value indicates the uncalibrated model overestimates the peak flow of the calibrated model. The distribution of peak flow percent errors has a mean of 14%, which suggests that the uncalibrated models are conservative on average. The standard deviation is 39%, which could be used to develop a factor of safety to reduce the likelihood that the uncalibrated models underestimate the peak flow.

4.4 Analysis of Time Constant Assumptions

In the proposed uncalibrated parameter estimation methods, the Clark time constant R and the groundwater time constants T_{GW} were assumed to be independent of sub-basin size (i.e. set to constants). This assumption can be tested by developing lumped models for the basins, using the lumped models to simulate the design storms, and comparing the results of the lumped models to the results of the semi-distributed models. Because the design storm rainfall is spatially constant across the basin, the lumped models should produce similar results to the semi-distributed models if the parameters properly account for the basin size.

In this experiment, two lumped models considered for each basin. One uses the proposed constant values for R and T_{GW} (i.e., the values remain the same as the semi-distributed models). The other uses $R = 3T_c$ and $T_{GW} = 12T_c$ (i.e., the values scale with basin size). T_c was calculated using Eq. 5. Fig. 10 shows that the lumped models with constant values produce better estimates of the semi-distributed results than the lumped models with values based on T_c. When the lumped models are created, the sub-basins and reaches are replaced with a single basin. The parameters of the single basin need to account for any attenuation in flow that occurs in the removed reach elements of the semi-distributed model. The constant values neglect any such attenuation. They work well because the Muskingum-Cunge method produces very little attenuation in the steep and shallow reaches (Lee and Yen, 1997; Lee and Chun, 2012).

4.5 Comparison to Independent Estimates of Peak Flows

In this section, the peak flows generated by the uncalibrated models for the design storms are compared to other, independent estimates of extreme flows. First, the model results are compared to StreamStats, which estimates the peak discharge for 2, 5, 10, 20, 50, 100, 200, and 500-yr return periods (Capesius and Stephens, 2009). The StreamStats estimates are representative of natural streamflow conditions in Colorado. They are produced by regional regression equations that use drainage area, mean watershed elevation, mean watershed slope, percentage of drainage area above 2,300 m, mean annual precipitation, and the 6-hr 100-yr precipitation from NOAA-Atlas 2 (Capesius and Stephens, 2009).

Figs. 11 and 12 show the StreamStats estimates along with the peak flow estimates from the uncalibrated models in the Front Range and San Juan Range, respectively. The uncalibrated models estimate lower peak flows than StreamStats for the 10-yr and 100-yr return periods. These peak flows are likely produced by the spring melt of mountain snowpack or a combination of rainfall and snowmelt (Jarrett and Tomlinson, 2000), and snowmelt is not considered by the uncalibrated models. Most of the 1,000-yr flows and 10,000-yr flows from the uncalibrated model applications are below the 500-yr flow from StreamStats. This either indicates that melting snowpack continues to play a significant role for these return periods or that the uncalibrated models are underestimating the flows at these return periods. Either way, it suggests that the uncalibrated models are not applicable for these return periods. For return periods larger than 10,000 yr, the slope of the peak flow versus return period curve increases, and the uncalibrated models predict flows above the Streamstats 500-yr flow. For the 48-hr storms, the break in slope coincides with the initiation of saturation-excess runoff. This phenomenon has also been observed by Kusumastuti et al. (2006).

Regional peak flow envelope curves provide another independent method to evaluate the estimates from the models. In Colorado, peak flow envelope curves are available for regions based on geography and elevation (Crippen, 1977; Jarrett and Tomlinson, 2000). For this study, the envelope originally developed by Crippen (1977) is used along with the peak flow measurements in the USGS Colorado Flood Database (Fig. 13). These data are typically used by

Colorado dam safety regulators as a reasonableness check for predicted peak flows. The Crippen (1977) envelope considers peak flows from mountainous areas > 2,300 m as well as lower elevation areas. Because lower elevations are known to experience more severe storms (Jarrett, 1993), the Crippen (1977) is expected to overestimate peak flows for mountainous areas. Fig. 13 also displays the maximum peak streamflow estimates for each basin from the calibrated and uncalibrated models. Most of the modeled flows are produced by the 2-hr, 6-hr, or 72-hr PMP event. The modeled peak streamflow estimates are above the observed peak flows at the associated drainage area, but below the envelope from Crippen (1977). The calibrated and uncalibrated models also produce similar results when viewed in the context of this plot.

5. DISCUSSION

Overall, promising results were obtained for modeling the response of ungauged mountain basins in Colorado to extreme precipitation. Colorado's existing hydrologic modeling guidelines neglect subsurface stormflow and saturation-excess runoff, which Woolridge et al. (2020) showed occurred for some historical storms. The proposed modeling approach can produce discharge from such mechanisms. Colorado's current modeling guidelines are also known to greatly overestimate major floods in the mountains (Jarrett, 1993; Perry et al., 2017). In contrast, the average NSCE of the proposed uncalibrated models is 0.61. For context, Razavi and Coulibaly (2013) evaluated the performance of uncalibrated models in studies across different regions and climates, and the average NSCE for the models in those studies is 0.61 with a range from 0.12 to 0.97. The proposed parameter estimation methods are also relatively simple to implement. Because no published guidance is available for SMA parameter estimation, the proposed methods might also provide insights for parameter estimation for regions outside of Colorado.

However, several limitations remain. The methods were developed and tested using basins from two mountain ranges in Colorado. Basins in central Colorado (such as the Gore, Sawatch, and Elk ranges) and western Colorado (such as the Flat Tops, Grand Mesa, and the Uncompahgre Plateau) were not considered due to lack of data for large events. Each range has distinct geologic, geomorphologic, and vegetation characteristics, which are expected to impact the performance of the proposed methods. Also, the proposed groundwater percolation rate differs between the Front Range and the San Juan Range. Appropriate values for this parameter in other mountain ranges are unknown. The proposed methods are not expected to apply to nonmountainous portions of Colorado such as the Eastern plains. Bedrock is often very deep in the plains (gNATSGO, 2020), so saturation excess runoff and subsurface stormflow are less likely.

Most historical storms considered in this study had long durations that produced subsurface stormflow and saturation-excess runoff. Only two short duration, high intensity storms producing infiltration-excess runoff were available (North Fork Big Thompson River 1976 and Saguache Creek 1999). For North Fork Big Thompson River 1976, an incomplete hydrograph prevents a detailed evaluation of the model. For Saguache Creek 1999, uncertainty in the precipitation estimates also posed difficulties in interpreting the results. Also, the performance of the uncalibrated models is worse for the shorter storms than the longer storms. Thus, substantial uncertainty remains in the simulation of short duration, high intensity storms.

Some parameters, such as canopy storage, Clark storage coefficient, groundwater time constants, and groundwater percolation rate, were set to fixed values based on their performance for the historical events. Continuing research should explore ways to estimate these from basin characteristics. An improved canopy storage could consider fractional vegetation cover, which is already used in the parameter estimation methods. Groundwater parameters could be better constrained by considering smaller storms. Smaller storms are less likely to produce surface runoff, so they cannot be used to constrain surface runoff related parameters. However, subsurface stormflow still occurs for these events, so the related parameters can be analyzed.

The uncalibrated modeling methods should be used in a way that considers the uncertainty in their results. Comparison and even calibration to independent streamflow estimates is recommended. The errors associated with the parameter estimation methods were examined by comparing the peak flows for the uncalibrated and calibrated models for the design storms. This distribution could be used to develop a factor of safety.

Impacts of climate change on basin hydrology were not considered. This study focused only on rainfall induced flooding in undisturbed mountain watersheds. Due in part to climate change, wildfires are increasing in frequency and size across the western United States (Brown et al., 2004; Abatzoglou and Kolden 2013). Wildfires alter the soil structure and increase water repellency, which increases runoff production for years (DeBano, 2000; Doerr et al., 2000). Rain on snow events are becoming more common in the western United States with climate change as well (Surfleet and Tullos, 2013). If rainfall occurs when snowpack is present, it can produce much larger flows due to abrupt melting of snow. These events have potentially occurred in Colorado (FEMA, 2010) but might become more common under the modified climate. Climate change could also change the temporal distribution of antecedent soil moisture, which has the potential to impact runoff production for a given event.

6. CONCLUSIONS

The purpose of this study was to develop modeling methods that can be used to simulate the response of ungauged mountain basins in Colorado to large storms. The study focuses on the SMA method in HEC-HMS, which was previously shown to reproduce the streamflow generation mechanisms for large storms in the Colorado Front Range (Woolridge et al., 2020). Seven historical storms that represent all four flood-generating storm types in REPS were simulated for five basins in the Front Range and three basins in the San Juan Range. The results from the proposed parameter estimation methods (i.e., the uncalibrated models) were compared to the observed streamflow hydrographs and the results from calibrated models. In addition, various duration AEP and PMP design storms from REPS were simulated for the same basins. The results from the uncalibrated models were compared to the results from the calibrated models, StreamStats, and a regional peak flow envelope. The following conclusions can be drawn from this study:

- The proposed model simplifications (merging of north-facing and south-facing hillslope elements and use of the default HEC-HMS time area curve) and parameter estimation methods perform well for the studied historical storms in the Front Range and San Juan Range. The average RMSE and NSCE for the uncalibrated models (excluding Saguache Creek 1999, which is considered an outlier) are 5.56 m^3/s and 0.65, respectively. For comparison, the average RMSE and NSCE for the calibrated models (excluding Saguache Creek 1999) are 4.55 m^3/s and 0.80, respectively. Saguache Creek 1999 is considered an outlier due to its anomalously low runoff coefficient and high uncertainty in its precipitation estimates.

- For all but one historical event, the uncalibrated models produce streamflow by the same mechanisms as the calibrated models. For the case where the mechanism changed (Cheyenne Creek 1997), the overall model performance of the uncalibrated model was better than the previously calibrated model.
- The primary sources of error in the uncalibrated models are the soil and groundwater parameters. The groundwater parameters describe the flow on top of the bedrock. They are the most poorly constrained due to limited information about the weathered bedrock surface where subsurface stormflow occurs.
- The uncalibrated models provide rough estimates of the peak flows from the calibrated models for the design storms in the studied basins. On average, the uncalibrated models overestimate the peak flows from the calibrated models by 14%. However, the standard deviation of the peak flow error is 39%. Thus, the predictions from the uncalibrated models are typically but not consistently conservative.
- The uncalibrated models do not produce accurate peak flows for return periods less than 1000 yr to 10,000 yr. For these return periods, the models produce lower peak flows than the regional regression equation in StreamStats. This underestimation likely occurs because the models neglect the contribution from spring melt of mountain snowpack, which plays a role in the small return period peak flows. For return periods at or above 10,000 yr, the peak flows from the models are usually much higher than the StreamStats 500-yr flows as expected.
- The uncalibrated models appear to produce reasonable results for very large storm events. The largest streamflow values from the uncalibrated models among all design storms are above all the observed peak flows in the USGS Colorado Flood Database. They are

below the envelope developed by Crippen (1977), which is expected because that envelope also considered lower elevations.

7. TABLES AND FIGURES

Table 1. Characteristics of the modeled Front Range and San Juan Range basins.

Range	Basin	Area (km^2)	Elevation Range (m)	Sub-Basins in Model
Front	North Fork Big Thompson River	220	1875 – 4150	9
	Big Thompson River	357	2284 – 4347	15
	South Boulder Creek	278	1900 – 4050	12
	Bear Creek	267	2157 – 4345	9
	Cheyenne Creek	56	1905 – 3770	3
San Juan	Mineral Creek	135	2820 – 4189	3
	Vallecito Creek	187	2414 – 4153	6
	Saguache Creek	1340	2448 – 4230	57

Table 2. Historical storm characteristics for each basin in the Front Range and San Juan Range. MEC denotes mesoscale storm with embedded convection, MLS denotes mid-latitude cyclone, LS denotes local storm, and TSR denotes tropical storm remnant. For Vallecito 2004, the highest observed streamflow was used to calculate the ratio with the StreamStats 100-yr flow (even though the actual peak flow may not have been recorded). Runoff coefficients were not calculated when the observed hydrographs were incomplete or had only daily average flows.

Basin and Storm Year	Storm Dates	Storm Type	Avg. Total Rainfall (mm)	Max. Total Rainfall (mm)	Ratio of Peak Flow to StreamStats 100-yr Flow	Runoff Coefficient
North Fork Big Thompson River 1976	7/31 – 8/1	MEC	79	300	3.5	-
Cheyenne Creek 1997	6/9 – 6/11	MLC	101	130	0.5	0.56
Big Thompson River 2013	9/9 – 9/16	MLC	182	240	1.3	0.23
South Boulder Creek 2013	9/9 – 9/16	MLC	150	325	1.5	0.28
Bear Creek 2013	9/9 – 9/16	MLC	195	220	1.4	0.26
Cheyenne Creek 2013	9/9 – 9/16	MLC	294	350	1.2	0.26
Vallecito Creek 1970	9/3 – 9/8	TSR	123	123	3.2	-
Saguache Creek 1999	7/25 – 7/26	LS	19	140	0.4	0.06
Mineral Creek 2004	9/18 – 9/24	TSR	95	104	0.7	0.27
Vallecito Creek 2004	9/18 – 9/24	TSR	101	128	0.9	-
Mineral Creek 2006	10/3 – 10/9	MLC	86	91	0.6	0.69
Vallecito Creek 2006	10/3 – 10/9	MLC	102	132	1.7	0.60

Table 3. Overall performance metrics for calibrated and uncalibrated models of the Front Range and San Juan Range basins. Root mean squared error (RMSE), Nash-Sutcliffe Coefficient of Efficiency (NSCE), and percent error in volume are not included for cases with incomplete observed hydrographs. A negative value of percent error in volume indicates an underestimation by the model. Saguache Creek 1999 is not included in the calculation of averages (see discussion in main text).

Storm	Basin	Runoff Mechanism		RMSE (m^3/s)		NSCE		Percent Error Volume (%)	
		Calib. model	Uncalib. model	Calib. model	Uncalib. model	Calib. model	Uncalib. model	Calib. model	Uncalib. model
1976	North Fork Big Thompson River	I-E	I-E	-	-	-	-	-	-
1997	Cheyenne Creek	Neither	S-E	1.74	1.68	0.71	0.73	7	-25
2013	Big Thompson River	S-E	S-E	7.34	6.80	0.89	0.91	3	-14
2013	South Boulder Creek	S-E	S-E	4.30	5.73	0.83	0.70	8	-3
2013	Bear Creek	Neither	Neither	4.91	6.20	0.83	0.72	23	-11
2013	Cheyenne Creek	S-E	S-E	4.40	4.50	0.68	0.67	27	6
1970	Vallecito Creek	S-E	S-E	-	-	-	-	-	-
1999	Saguache Creek	I-E	I-E	6.68	65.57	-0.07	-102.7	50	562
2004	Mineral Creek	S-E	S-E	4.19	8.17	0.75	-0.12	19	55
2004	Vallecito Creek	S-E	S-E	-	-	-	-	-	-
2006	Mineral Creek	S-E	S-E	3.91	4.02	0.80	0.68	-15	9
2006	Vallecito Creek	S-E	S-E	5.62	7.39	0.93	0.89	-1	6
	Average	-	-	4.55	5.56	0.80	0.65	9	3

Table 4. Peak flow performance metrics for calibrated and uncalibrated models of the Front Range and San Juan Range basins. For the Front Range basins, calibrated models are from Woolridge et al. (2020). A negative value of peak flow error, percent error in peak flow, and percent error in time to peak indicates an underestimation by the model. Saguache Creek 1999 is not included in the calculation of averages.

Storm	Basin	Peak Flow Error (m^3/s)		Percent Error in Peak Flow (%)		Percentage Error in Time to Peak (%)	
		Calib. model	Uncalib. model	Calib. model	Uncalib. model	Calib. model	Uncalib. model
1976	North Fork Big Thompson River	3.4	60.9	1	25	25.0	50.0
1997	Cheyenne Creek	-6.4	-2.0	-38	-12	23.1	-1.3
2013	Big Thompson River	-0.6	9.3	-1	11	-0.4	-3.4
2013	South Boulder Creek	-22.8	-9.9	-32	-14	1.1	-19.8
2013	Bear Creek	-2.8	-0.7	-7	-2	5.0	5.2
2013	Cheyenne Creek	-8.5	9.9	-20	24	2.3	-0.4
1970	Vallecito Creek	39.1	11.1	20	6	-	-
1999	Saguache Creek	6.2	240.1	10	394	0.0	0.0
2004	Mineral Creek	-8.0	-3.7	-22	-10	-0.2	-0.2
2004	Vallecito Creek	8.0	3.2	15	6	-14.0	-14.2
2006	Mineral Creek	-0.4	4.1	-1	13	-1.7	-2.3
2006	Vallecito Creek	10.8	5.9	10	6	-0.4	-0.4
	Average	1.07	8.01	-6.82	4.82	4.0	1.3

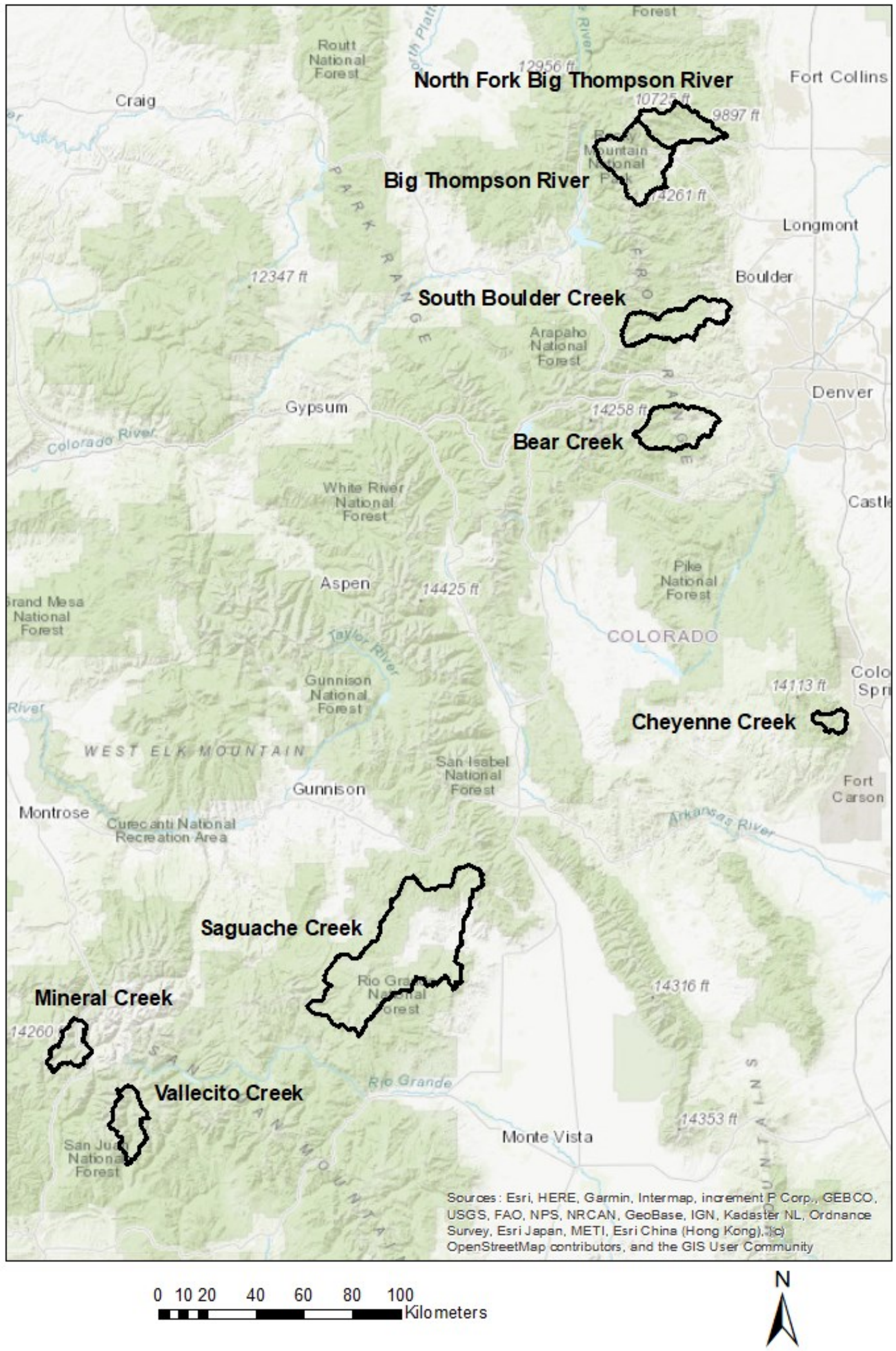

Figure 1. Study basins in the Front Range west of Denver and the San Juan Range west of Monte Vista.

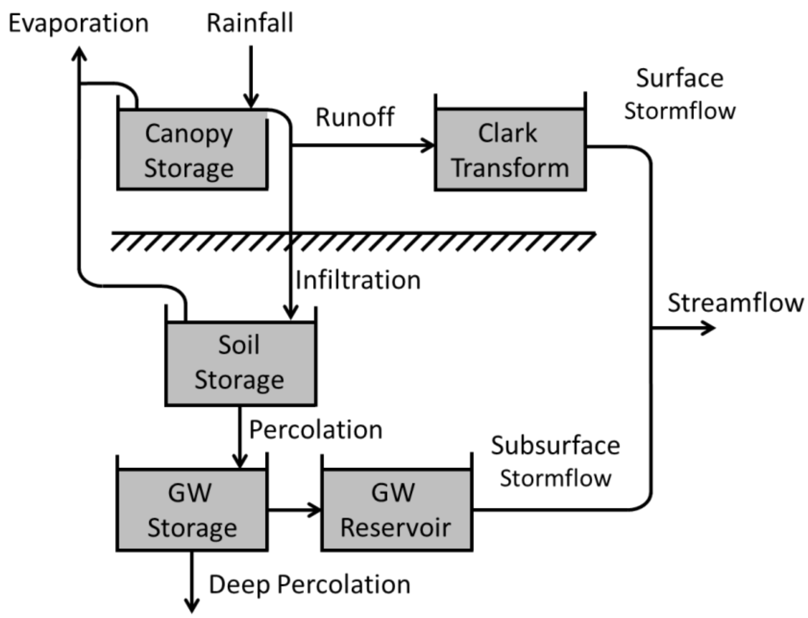

Figure 2. Schematic diagram of the model components.

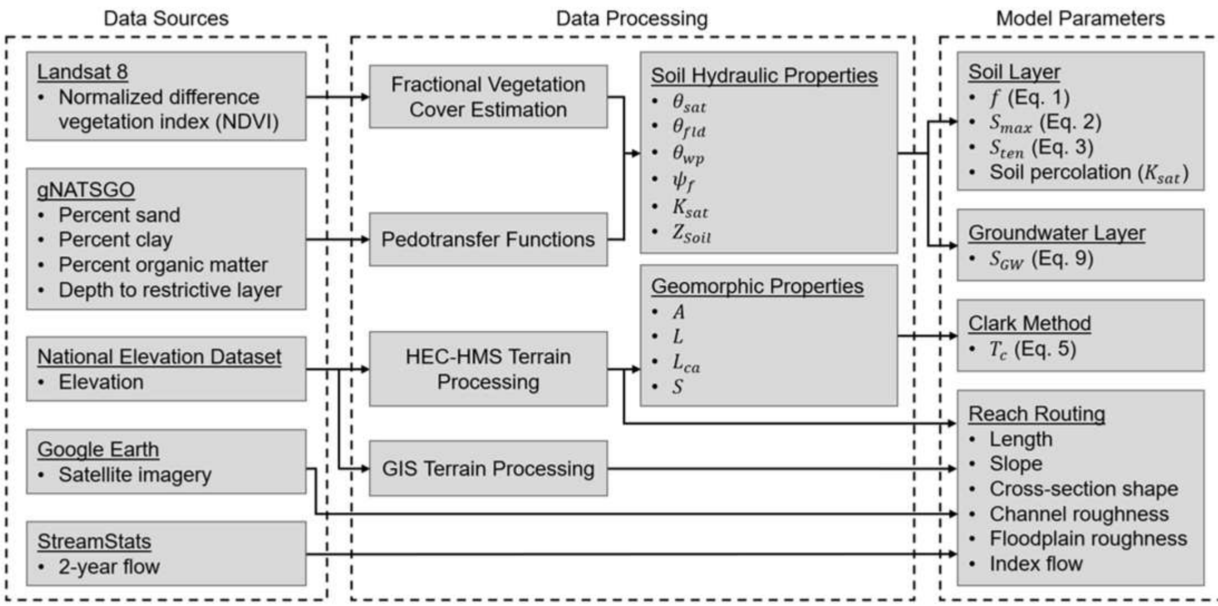

Figure 3. Summary of proposed parameter estimation procedure.

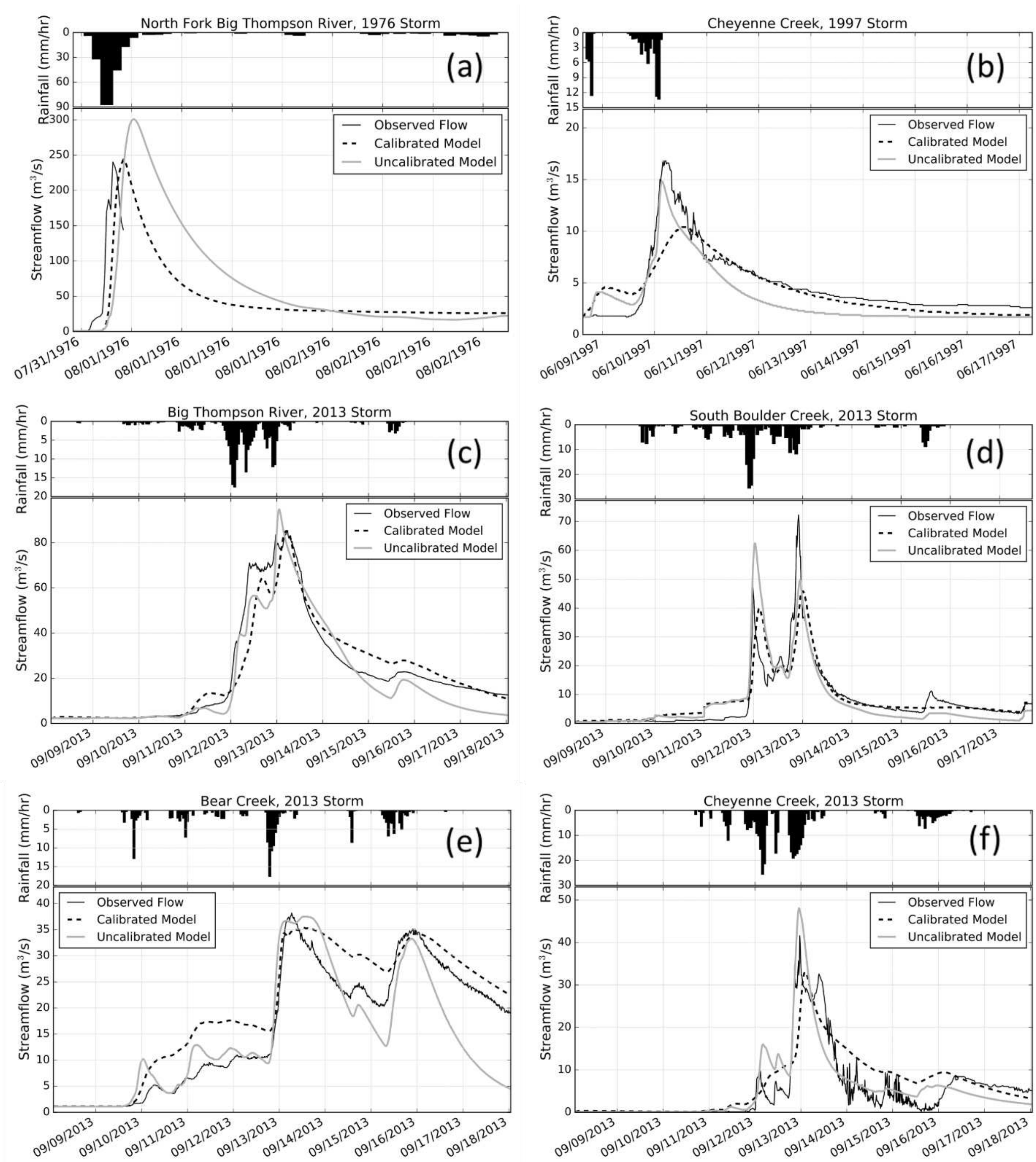

Figure 4. Observed spatial average rainfall intensity and comparison of observed and modeled streamflow for Front Range basins: (a) North Fork Big Thompson River 1976, (b) Cheyenne Creek 1997, (c) Big Thompson River 2013, (d) South Boulder Creek 2013, (e) Bear Creek 2013, and (f) Cheyenne Creek 2013.

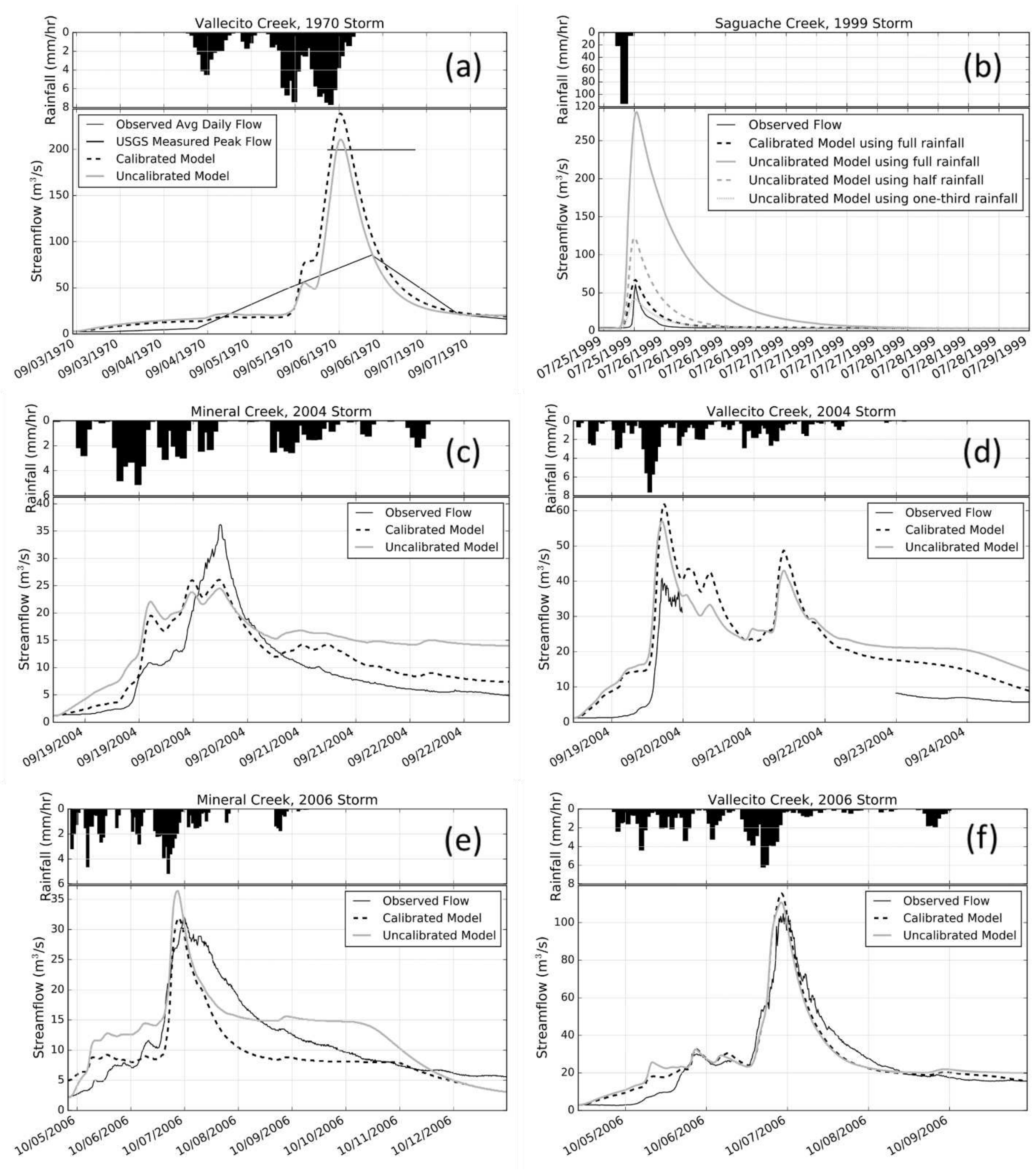

Figure 5. Observed spatial average rainfall intensity and comparison of observed and modeled streamflow for San Juan Range basins: (a) Vallecito Creek 1970, (b) Saguache Creek 1999, (c) Mineral Creek 2004, (d) Vallecito Creek 2004, (e) Mineral Creek 2006, and (f) Vallecito Creek 2006.

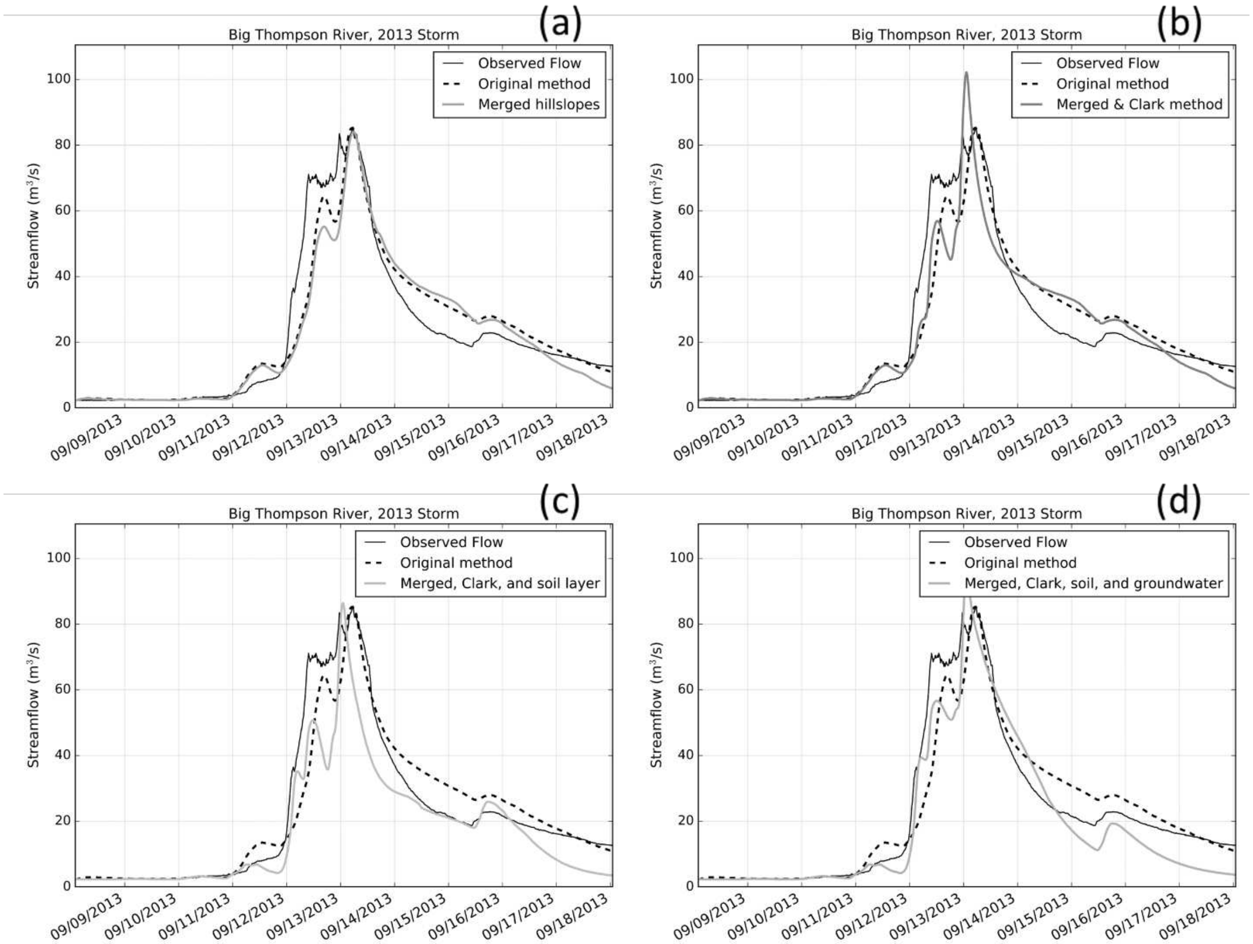

Figure 6. Results incrementally changing the parameter values beginning with the calibrated model and progressing towards the uncalibrated model for the Big Thompsons River 2013 event.

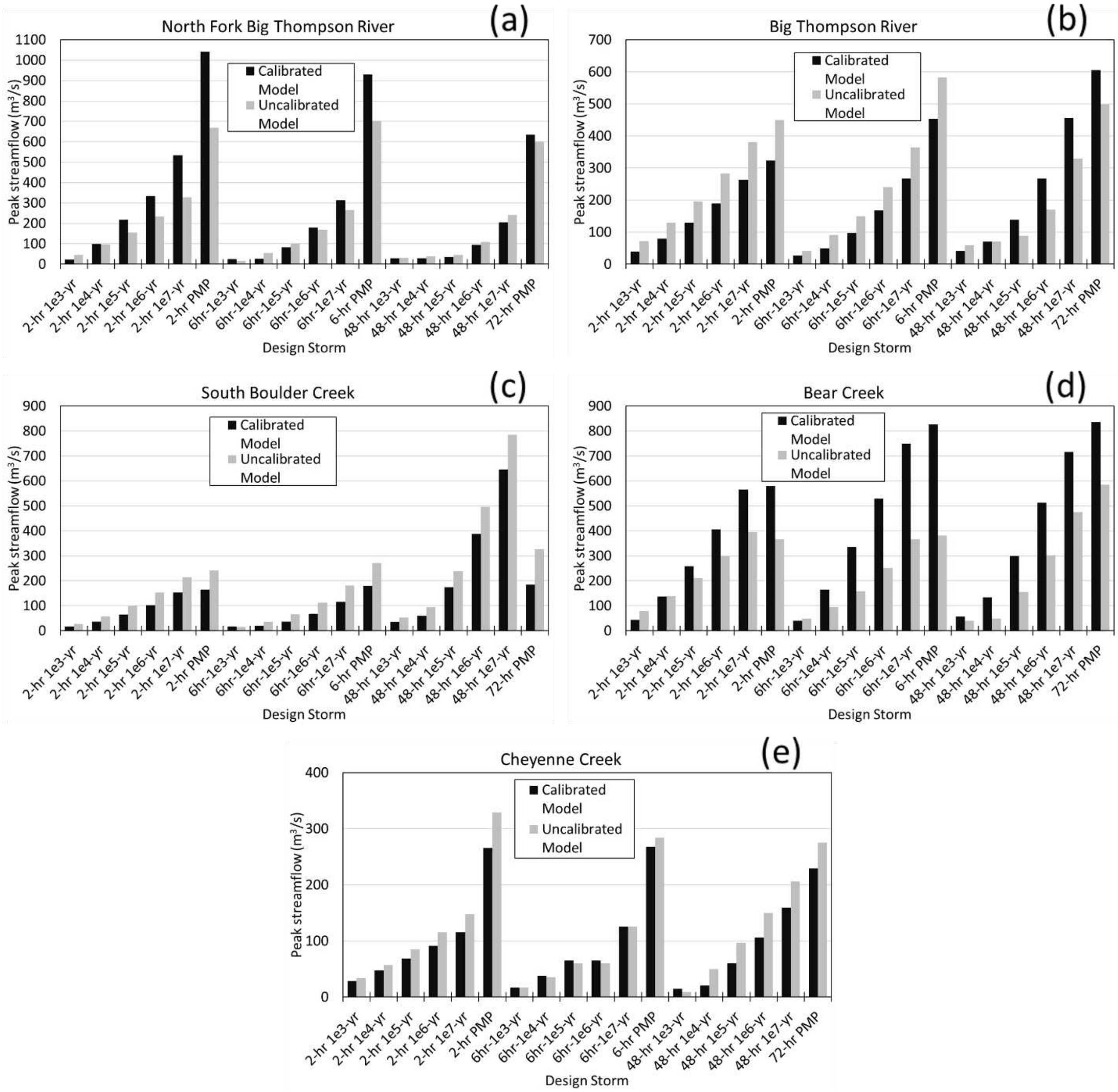

Figure 7. Peak streamflow values generated by the calibrated and uncalibrated models for design storms in the Front Range basins: (a) North Fork Big Thompson River, (b) Big Thompson River, (c) South Boulder Creek, (d) Bear Creek, and (e) Cheyenne Creek.

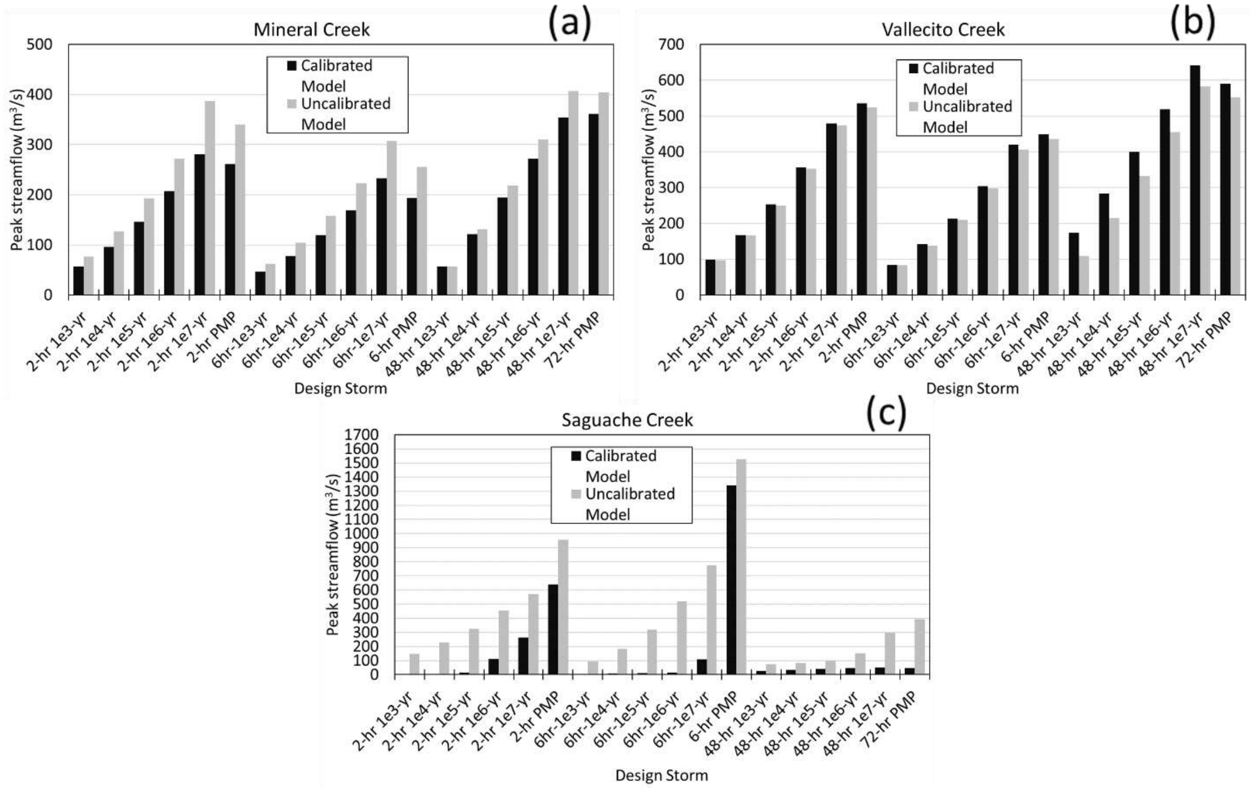

Figure 8. Peak streamflow values generated by the calibrated and uncalibrated models for design storms in the San Juan Range basins: (a) Mineral Creek, (b) Vallecito Creek, and (c) Saguache Creek.

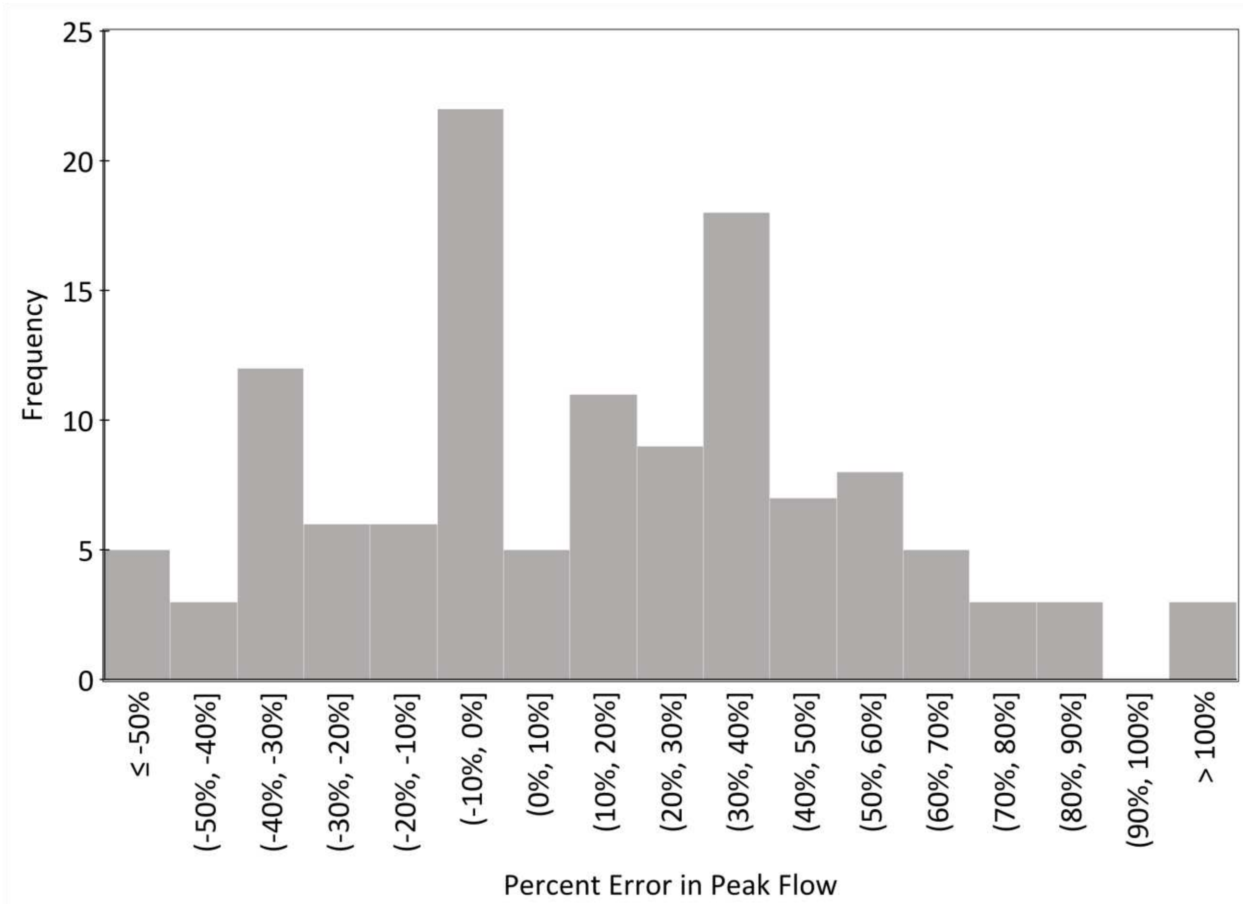

Figure 9. Histogram of percent error in peak flow from the uncalibrated model when applied to all basins and design storms.

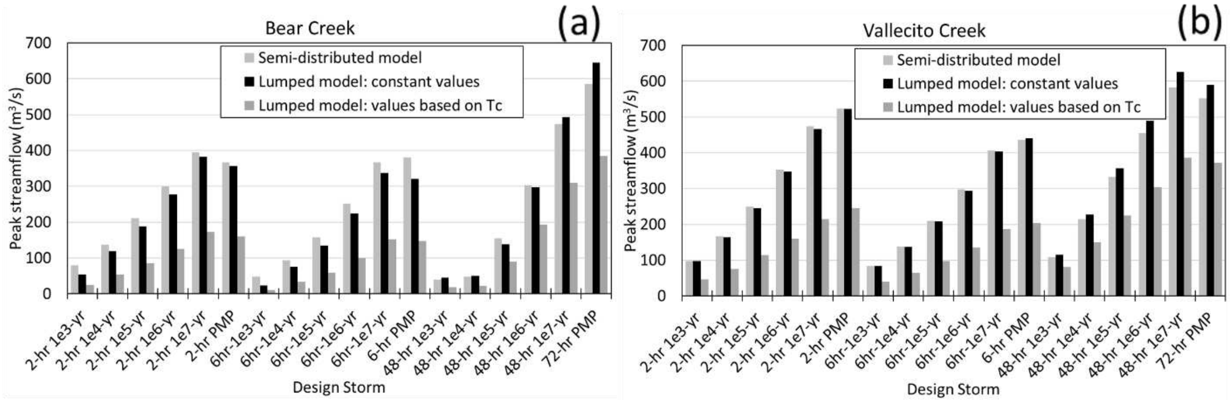

Figure 10. Peak streamflow values generated by semi-distributed and lumped uncalibrated models: (a) Bear Creek and (b) Vallecito Creek.

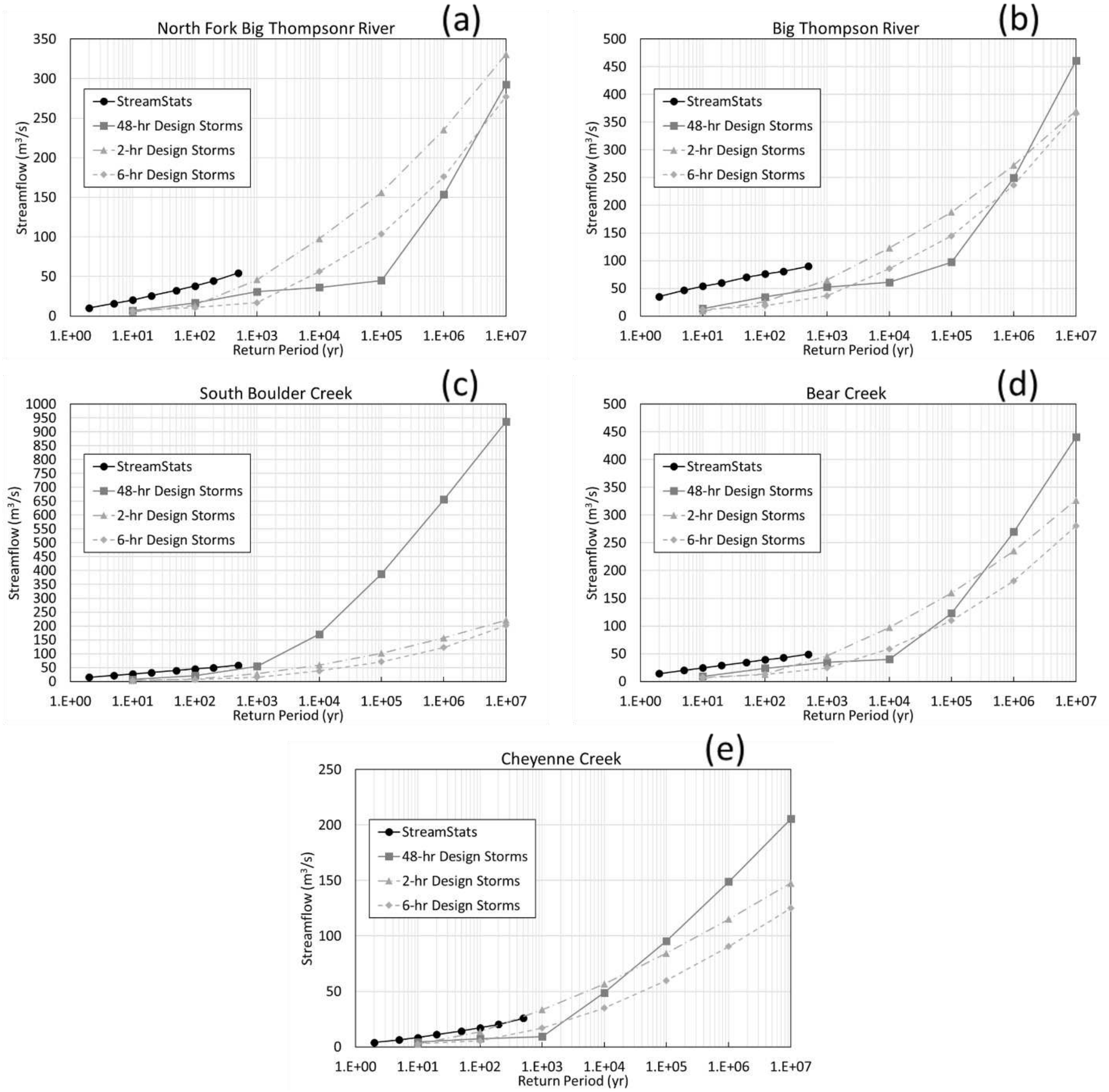

Figure 11. Design storm peak flow comparison between StreamStats and uncalibrated models for Front Range basins: (a) North Fork Big Thompson River, (b) Big Thompson River, (c) South Boulder Creek, (d) Bear Creek, (e) Cheyenne Creek.

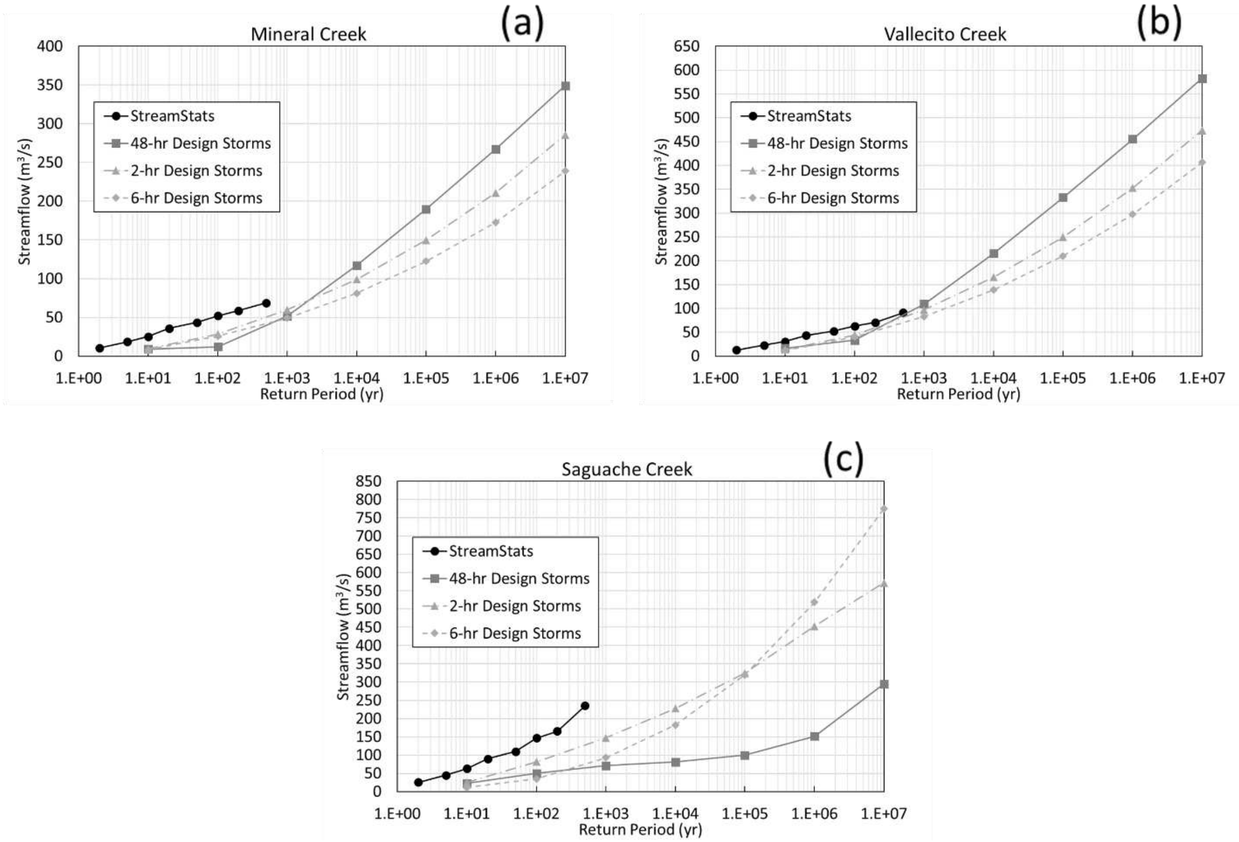

Figure 12. Design storm peak flow comparison between StreamStats and uncalibrated models for San Juan Range basins: (a) Mineral Creek, (b) Vallecito Creek, (c) Saguache Creek.

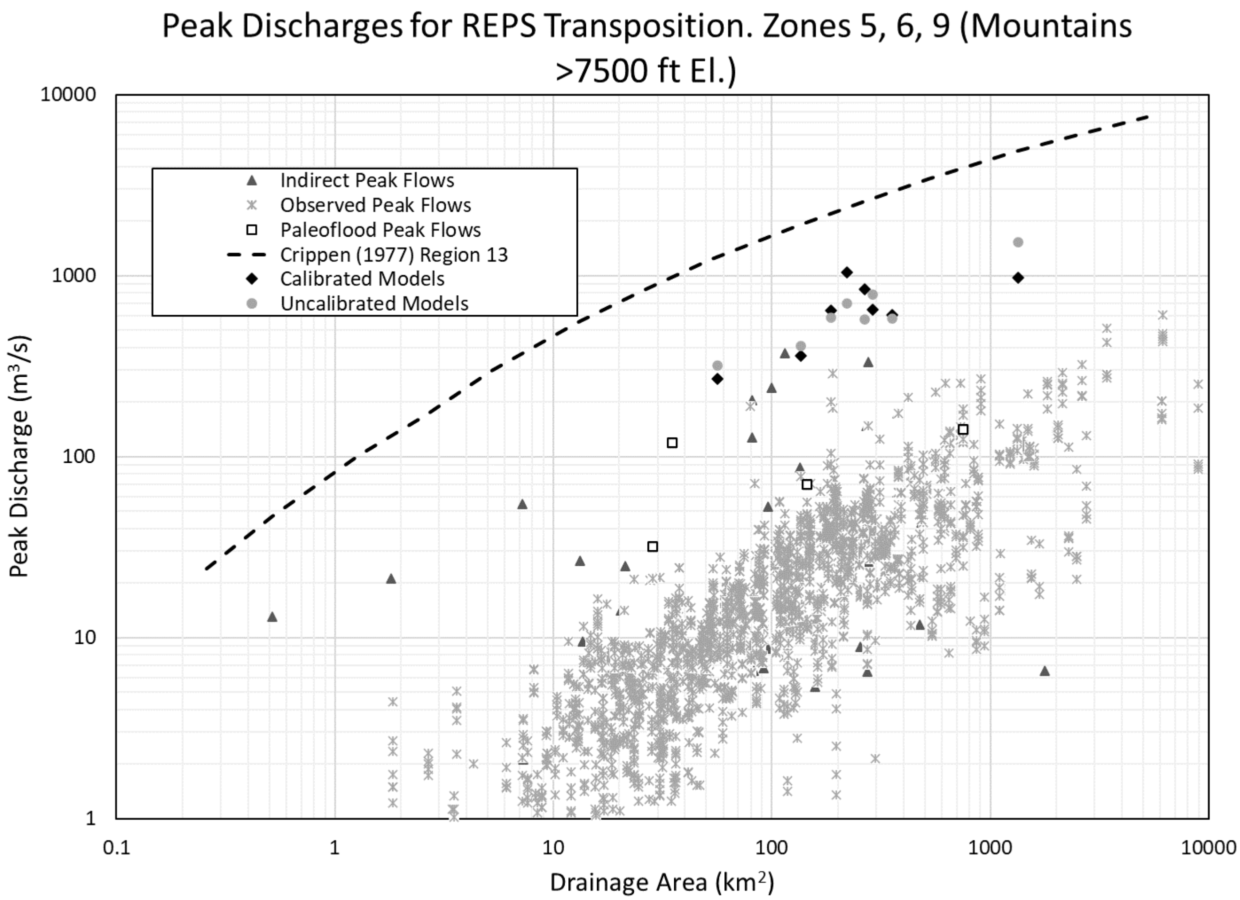

Figure 13. Regional peak flow envelope from Crippen (1977), observed peaks flows for Colorado mountain basins (USGS Colorado Flood Database (1/20/2021), and the largest peak flows from the calibrated and uncalibrated models from the design storms.

REFERENCES

Abatzoglou, John T., and Crystal A. Kolden (2013). “Relationships between Climate And Macroscale Area Burned in the Western United States.” International Journal of Wildland Fire, vol. 22, no. 7, p. 1003., doi:10.1071/wf13019.

Ahl, Robert S., Woods, Scott W., Zuuring, Hans R. (2008). “Hydrologic Calibration and Validation of SWAT in a Snow-Dominated Rocky Mountain Watershed, Montana, U.S.A.1.” JAWRA Journal of the American Water Resources Association, vol. 44, no. 6, pp. 1411–1430., doi:10.1111/j.1752-1688.2008.00233.x.

Almeida, I.K., Almeida, A.K., Anache, J.A.A., Steffen, J.L., T. Alves Sobrinho (2014). “Estimation of time of concentration in overland flow in watersheds: a review.” São Paulo, UNESP, Geociências, 33 (4), pp. 661-671

Anderson, Scott W., Anderson, Suzanne P., Anderson, Robert S. (2015),“Exhumation by Debris Flows in the 2013 Colorado Front Range Storm.” Geology, vol. 43, no. 5, pp. 391–394., doi:10.1130/g36507.1.

Anderson, S. P., Hinckley, E.-L., Rock, N., and Ragar, D. (2019). “CZO Dataset: Gordon Gulch: Lower - Soil Temperature, Soil Moisture (2009-2019) - Soil Sensors (GGL)SPTran_SLTmpSLMist_Array).” Boulder Creek Critical Zone Observatory, <http://criticalzone.org/boulder/data/dataset/2426/> (Jun. 11, 2017).

Andréassian, Vazken, Oddos, Audrey, Michel, Claude, Anctil, Francois, Perrin, Charles, Loumagne, Cécile (2004). “Impact of Spatial Aggregation of Inputs and Parameters on the Efficiency of Rainfall-Runoff Models: A Theoretical Study Using Chimera Watersheds.” Water Resources Research, vol. 40, no. 5, doi:10.1029/2003wr002854.

Bennett, Todd H. (1998). “Development and Application of a Continuous Soil Moisture

Accounting Algorithm for the Hydrologic Engineering Center Hydrologic Modeling System (HEC-HMS).” Thesis (M.S.), University of California, Davis, 1998.

Bennett, Todd H., and John C. Peters (2000). “Continuous Soil Moisture Accounting in the Hydrologic Engineering Center Hydrologic Modeling System (HEC-HMS).” Building Partnerships, doi:10.1061/40517(2000)149.

Beven, Keith (1993). “Prophecy, Reality and Uncertainty in Distributed Hydrological Modelling.” Advances in Water Resources, vol. 16, no. 1, pp. 41–51., doi:10.1016/0309-1708(93)90028-e.

Blöschl, G., and M. Sivapalan (1995). “Scale Issues in Hydrological Modelling: A Review.” Hydrological Processes, vol. 9, no. 3-4, pp. 251–290., doi:10.1002/hyp.3360090305.

Bouwer, H. (1964). “Unsaturated flow in ground-water hydraulics.” *J. Hydraul. Div.* 90 (5): 121–144.

Brown, Timothy J., Hall, Beth L., Westerling, Anthony L. (2004). “The Impact of Twenty-First Century Climate Change On Wildland Fire Danger in the Western United States: An Applications Perspective.” Climatic Change, vol. 62, no. 1-3, pp. 365–388., doi:10.1023/b:clim.0000013680.07783.de.

Burnash RJC (1995) “The NWS river forecast system: catchment modeling. In: Singh VP (ed) Computer models of watershed hydrology.” Water Resources, Littleton, CO, pp 311–366

Caldwell, Peter V., Kennen, Jonathan G., Sun, Ge, Kiang, Julie E., Butcher, Jon B., Eddy, Michele C., Hay, Lauren E., LaFontaine, Jacob H., Hain, Ernie F., Nelson, Stacy A.C., McNulty, Steve G. (2015). “A Comparison of Hydrologic Models for Ecological Flows and Water Availability.” Ecohydrology, vol. 8, no. 8, pp. 1525–1546., doi:10.1002/eco.1602.

Capesius, J. P., and Stephens, V. C. (2009). “Regional Regression Equations for Estimation of

Natural Streamflow Statistics in Colroado Scientific Investigations Report 2009-5136.” Reston, VA.

Chimner, Rod A., Lemly, Joanna M., Cooper, David J. (2010). “Mountain Fen Distribution, Types and Restoration Priorities, San Juan Mountains, Colorado, USA.” Wetlands, vol. 30, no. 4, pp. 763–771., doi:10.1007/s13157-010-0039-5.

Chow, V. Te. (1959). Open-Channel Hydraulics. (H. E. Davis, ed.), McGraw-Hill Book Company, Inc.

Clark, C. O. (1945). “Storage and the unit hydrograph.” American Society of Civil Engineers Transactions, 2261, 1410–1446.

Cotton, W. R., McAnelly, R.L., Ashby, T. (2003), “Development of New Methodologies for Determining Extreme Rainfall.” Report, Department of Natural Resources, Colorado State University, Fort Collins, CO.

Crippen, John R. (1977). “Maximum Floodflows in the Conterminous United States.” Geological Survey Water-Supply Paper, no. 1887, doi:10.3133/wsp1887.

DeBano, L.F. (2000).“The Role of Fire and Soil Heating on Water Repellency in Wildland Environments: A Review.” Journal of Hydrology, vol. 231-232, pp. 195–206., doi:10.1016/s0022-1694(00)00194-3.

Dickinson, William R., Klute, Margaret A., Hayes, Michael J., Janecke, Susanne U., Lundin, Erik R., McKittrick, Mary A., Olivares, Mark D. (1988). “Paleogeographic and Paleotectonic Setting of Laramide Sedimentary Basins in the Central Rocky Mountain Region.” Geological Society of America Bulletin, vol. 100, no. 7, pp. 1023–1039., doi:10.1130/0016-7606(1988)100<1023:papsol>2.3.co;2.

Din SU, Khan NM, Israr M, Nabi H, Khan M (2019). “Runoff modelling using HEC-HMS for rural watershed." Int J AdvEng Res Dev 6(12):79–85

Djokic, D., Z. Ye, and C. Dartiguenave. (2011). Arc hydro tools overview version 2.0. Redlands, CA: Esri.

Doerr, S.H., Shakesby, R.A., Walsh, R.P.D. (2000). "Soil Water Repellency: Its Causes, Characteristics and Hydro-Geomorphological Significance." Earth-Science Reviews, vol. 51, no. 1-4, pp. 33–65., doi:10.1016/s0012-8252(00)00011-8.

Dunn, C., Hurst, M., Dotson, H., McPherson, M., Doan, J., and Evans, T. (2001). "HEC-HMS for the Sacramento and San Joaquin River Basins Comprehensive Study." Sacramento, CA.

Dunne, Thomas, and Richard D. Black. (1970a). "Partial Area Contributions to Storm Runoff in a Small New England Watershed." Water Resources Research, vol. 6, no. 5, pp. 1296–1311., doi:10.1029/wr006i005p01296.

Dunne, Thomas, and Richard D. Black. (1970b). "An Experimental Investigation of Runoff Production in Permeable Soils." Water Resources Research, vol. 6, no. 2, pp. 478–490., doi:10.1029/wr006i002p00478.

Ebel, Brian A. (2012)."Wildfire Impacts on Soil-Water Retention in the Colorado Front Range, United States." Water Resources Research, vol. 48, no. 12, doi:10.1029/2012wr012362.

Feldman, A. D. (2000). Hydrologic Modeling System Technical Reference Manual. Institute for Water Resources, Hydrologic Engineering Center, Davis, CA.

FERC (Federal Energy Regulatory Commission). (2001). Engineering guidelines for the evaluation of hydropower projects: Assessment. Washington, DC: FERC.

Flood Insurance Study: La Plata County Colorado, and Incorporated Areas, FEMA, 2010.

Folmar, Norman D., Miller, Arthur C., Woodward, Donald E. (2007). "History and Development of the NRCS Lag Time Equation." Journal of the American Water Resources Association, vol. 43, no. 3, pp. 829–838., doi:10.1111/j.1752-1688.2007.00066.x.

Freer, Jim, McDonnell, J.J., Beven, K.J., Peters, N.E., Burns, D.A., Hooper, R.P., Aulenbach, B., Kendall, C. (2002). "The Role of Bedrock Topography on Subsurface Storm Flow." Water Resources Research, vol. 38, no. 12, doi:10.1029/2001wr000872.

Freeze, R. Allan. (1972). "Role of Subsurface Flow in Generating Surface RUNOFF: 2. Upstream Source Areas." Water Resources Research, vol. 8, no. 5, 1972, pp. 1272–1283., doi:10.1029/wr008i005p01272.

Gochis, D., Schumacher, R., Friedrich, K., Doesken, N., Kelsch, M., Sun, J., Ikeda, K., Lindsey, D., Wood, A., Dolan, B., Matrosov, S., Newman, A., Mahoney, K., Rutledge, S., Johnson, R., Kucera, P., Kennedy, P., Sempere-Torres, D., Steiner, M., Roberts, R., Wilson, J., Yu, W., Chandrasekar, V., Rasmussen, R., Anderson, A., and Brown, B. (2015). "The great Colorado flood of September 2013." Bulletin of the American Meteorological Society, 96(9), 1461–1487.

Google. (2020). [Google Earth view of Colorado Rocky Mountain watersheds]. Retrieved October 15, 2020, from https://earth.google.com/web/@40.34118063,-105.5568299,2663.8701162a,6744.69921409d,35y,0h,0t,0r

Green, W. H., and Ampt, G. A. (1911). "Studies on Soil Physics, part 1 - the flow of air and water through soils." The Journal of Agricultural Science, 4(1), 1–24.

Hallema, Dennis W., Moussa, Roger, Sun, Ge, McNulty, Steven G. (2016). "Surface Storm Flow Prediction on Hillslopes Based on Topography and Hydrologic Connectivity." Ecological Processes, vol. 5, no. 1, doi:10.1186/s13717-016-0057-1.

Heiss, W., D. McGrew, and D. Sirmans. (1990). "NEXRAD: Next Generation Weather Radar (WSR-88D)". Microwave Journal.,33, 79–98.

Henz, John. (2001). “Radar-Rainfall Reconstruction of The Saguache Creek Flash Flood of July 25, 1999”, by HDR Hydro-Meteorological Services (HMS) for Colorado Water Conservation Board, June 2001.

Horton, R. E. (1940). “An Approach Toward a Physical Interpretation of Infiltration-Capacity1.” Soil Science Society of America Journal, 5, 399–417.

Hubbert, J., and F. Pratte. (2006). “Differential Reflectivity Calibration For Nexrad.” 2006 IEEE International Symposium on Geoscience and Remote Sensing, doi:10.1109/igarss.2006.138.

Jarrett, R. D., (1993). Flood Elevation Limits in the Rocky Mountains. In: Engineering Hydrology, C. Y. Kuo (Editor). Proceedings of the Symposium Sponsored by the Hydraulics Division of the American Society of Civil Engineers, pp. 180-185.

Jarrett, Robert D., and Edward M. Tomlinson (2000). “Regional Interdisciplinary Paleoflood Approach to Assess Extreme Flood Potential.” Water Resources Research, vol. 36, no. 10, 2000, pp. 2957–2984., doi:10.1029/2000wr900098.

Kampf, Stephanie K., and Stephen J. Burges. (2007) “A Framework for Classifying and Comparing Distributed Hillslope and Catchment Hydrologic Models.” Water Resources Research, vol. 43, no. 5, doi:10.1029/2006wr005370.

Kirkby, M. J., and Chorley, R. J. (1967). “Throughflow, overland flow and erosion.” Hydrological Sciences Journal, 12(3), 5–21., doi:10.1080/02626666709493533.

Kirkby, Michael John. Hillslope Hydrology. J. Wiley & Sons, 1989.

Kirpich, T.P. (1940). “Time of Concentration of Small Agricultural Watersheds.” Journal of Civil Engineering, v.10, n.6, p. 362.

Kitchen, M., and P. M. Jackson. (1993). “Weather Radar Performance at Long Range: Simulated and Observed.” Journal of Applied Meteorology, vol. 32, no. 5, pp. 975–985., doi:10.1175/1520-0450(1993)032<0975:wrpalr>2.0.co;2.

Kokkonen, Teemu S., Jakeman, Anthony J., Young, Peter C., Koivusalo, Harri J. (2003). “Predicting Daily Flows in Ungauged Catchments: Model Regionalization from Catchment Descriptors at THE Coweeta Hydrologic Laboratory, North Carolina.” Hydrological Processes, vol. 17, no. 11, pp. 2219–2238., doi:10.1002/hyp.1329.

Koren, V. I., M. Smith, D. Wang, and Z. Zhang (2000), “Use of soil property data in the derivation of conceptual rainfall-runoff model parameters.” paper presented at 15th Conference on Hydrology, Am. Meteorol. Soc.,Long Beach, Calif., 10 – 14 Jan.

Kusumastuti, D. I., Struthers, I., Sivapalan, M., Reynolds, D.A. (2006). “Threshold Effects in Catchment Storm Response and the Occurrence and Magnitude of Flood Events: Implications for Flood Frequency.” doi:10.5194/hessd-3-3239-2006.

Lee, Kwan Tun, and Ben Chie Yen. (1997). “Geomorphology and Kinematic-Wave–Based Hydrograph Derivation.” Journal of Hydraulic Engineering, vol. 123, no. 1, pp. 73–80., doi:10.1061/(asce)0733-9429(1997)123:1(73).

Lee, Kwan Tun, and Pin-Chun Huang. (2012). “Evaluating the Adequateness of Kinematic-Wave Routing for Flood Forecasting in Midstream Channel Reaches of Taiwan.” Journal of Hydroinformatics, vol. 14, no. 4, pp. 1075–1088., doi:10.2166/hydro.2012.093.

Linsley, Ray K., et al. (1992). Hidrología Para Ingenieros. Mc Graw-Hill, 1992.

McCain, J. F., Hoxit, L. R., Maddox, R. A., Chappell, C. F., and Caracena, F. (1979). “Storm and Flood of July 31-August 1, 1976 in the Big Thompson River and Cache la Poudre River Basins, Larimer and Weld Counties, Colorado, Part A. Meteorology and Hydrology in Big Thompson River and Cache la Poudre River Basins.” US Geological Survey Professional Paper 1115.

McIntyre, Neil, Lee, Hyosang, Wheater, Howard, Young, Andy, Wagener, Thorsten. (2005). “Ensemble Predictions of Runoff in Ungauged Catchments.” Water Resources Research, vol. 41, no. 12, doi:10.1029/2005wr004289.

MetStat. (2018). “Storm Precipitation Analysis System (SPAS).” <https://metstat.com/storm-analysis/spas/> (Aug. 16, 2018).

Montandon, L. M., and Small, E. E. (2008). “The impact of soil reflectance on the quantification of the green vegetation fraction from NDVI.” Remote Sensing of Environment, 112(4), 1835–1845., doi: 10.1016/j.rse.2007.09.007.

Moriasi, D. N., Arnold, J. G., Van Liew, M. W., Bingner, R. L., Harmel, R. D., and Veith, T. L. (2007). “Model evaluation guidelines for systematic quantification of accuracy in watershed simulations.” American Society of Agricultural and Biological Engineers, 50(3), 885–900., doi: 10.13031/2013.23153.

Parzybok, T.W. and E.M. Tomlinson. (2006). “A New System for Analyzing Precipitation from Storms.” *Hydro Review* 25: 58-65.

Pereira LS, Keller HM (1982). ”Factors affecting recession parameters and flow components in eleven small Pre-Alp basins.” IAHS Publ 138:233–242.

Perry, M. A., Franz, J., Dick, C., and Kappel, B. (2017). “Advances in Flood Hydrology for Modeling High Elevation Mountain Basins in Colorado with Applications to the Gross Dam Enlargement Study.” Association of State Dam Safety Officials Dam Safety Conferece, Philadelphia, Pennslyvania.

Petliak, Helen, Cerovski-Darriau, Corina, Zaliva, Vadim, Stock, Jonathan. (2019). “Where’s the Rock: Using Convolutional Neural Networks to Improve Land Cover Classification.” Remote Sensing, vol. 11, no. 19, p. 2211., doi:10.3390/rs11192211.

Rawls, W. J., Brakensiek, D. L., and Miller, N. (1983). “Green-ampt Infiltration Parameters from Soils Data.” Journal of Hydraulic Engineering, 109(1), 62–70., doi: 10.1061/(asce)0733-9429(1983)109:1(62).

Razavi, T. and P. Coulibaly. (2013). “Streamflow Prediction in Ungauged Basins: Review of Regionalization Methods.” Journal of Hydrologic Engineering, 18(8):958-975., doi: 10.1061/(asce)he.1943-5584.0000690.

Reed, Seann, Koren, Viktor, Smith, Michael, Zhang, Ziya, Moreda, Fekadu, Seo, Dong-Jun, and DMIP Participants. (2004). “Overall Distributed Model Intercomparison Project Results.” Journal of Hydrology, vol. 298, no. 1-4, pp. 27–60., doi:10.1016/j.jhydrol.2004.03.031.

Sabol, G. V. (2008). Hydrologic Basin Response Parameter Estimation Guidelines. State of Colorado, Office of the State Engineer, Dam Safety Branch.

Samper, Javier, Pisani, Bruno, Marques, Jorge E. (2014). “Hydrological Models of Interflow in Three Iberian Mountain Basins.” Environmental Earth Sciences, vol. 73, no. 6, pp. 2645–2656., doi:10.1007/s12665-014-3676-9.

Samuel, Jos, Coulibaly, Paulin, Metcalfe, Robert A. (2011). “Estimation of Continuous Streamflow in Ontario Ungauged Basins: Comparison Of Regionalization Methods.” Journal of Hydrologic Engineering, vol. 16, no. 5, pp. 447–459., doi:10.1061/(asce)he.1943-5584.0000338.

Saxton, K. E., and Rawls, W. J. (2006). “Soil Water Characteristic Estimates by Texture and Organic Matter for Hydrologic Solutions.” Soil Science Society of America Journal, 70, 1569–1578., doi: 10.2136/sssaj2005.0117.

Smith, James A., Seo, Dong Jun, Baeck, Mary Lynn, Hudlow, Michael D. (1996). “An Intercomparison Study of Nexrad Precipitation Estimates.” Water Resources Research, vol.

32, no. 7, pp. 2035–2045., doi:10.1029/96wr00270.

Soil Survey Staff. The Gridded National Soil Survey Geographic (gNATSGO) Database for Colorado. United States Department of Agriculture, Natural Resources Conservation Service. Available online at https://nrcs.app.box.com/v/soils. December 1, 2020 (FY2020 official release).

Sorooshian, Soroosh, Duan, Qingyun, Gupta, Vijai Kumar. (1993). "Calibration of Rainfall-Runoff Models: Application of Global Optimization to the Sacramento Soil Moisture Accounting Model." *Water Resources Research*, vol. 29, no. 4, pp. 1185–1194., doi:10.1029/92wr02617.

Surfleet, Christopher G., and Desirèe Tullos. (2013). "Variability in Effect of Climate Change ON Rain-on-Snow Peak Flow Events in a Temperate Climate." Journal of Hydrology, vol. 479, pp. 24–34., doi:10.1016/j.jhydrol.2012.11.021.

Timilsina, Sujana, Niemann, Jeffrey D., Rathburn, Sara L., Rengers, Francis K., Nelson, Peter A. (2021). "Modeling Hydrologic Processes Associated with Soil Saturation and Debris Flow Initiation during the September 2013 Storm, Colorado Front Range." Landslides, vol. 18, no. 5, pp. 1741–1759., doi:10.1007/s10346-020-01582-5.

Traff, D. C., Niemann, J. D., Middlekauff, S. A., and Lehman, B. M. (2015). "Effects of woody vegetation on shallow soil moisture at a semiarid montane catchment." Ecohydrology, 8(5), 935–947., doi: 10.1002/eco.1542.

Tweto, O., Geologic map of Colorado U.S. Geol. Surv., Denver Colorado, 1 (1979), p. 50 000

U.S. Geological Survey, (2020a). 3D Elevation Program 1/3 arc-second Resolution Digital Elevation Model (published 20150717), accessed October 15, 2020 at URL https://www.usgs.gov/core-science-systems/ngp/3dep/data-tools.

U.S. Geological Survey, (2020b). Department of the Interior. LANDSAT-8, OLI/TIRS C2 L2. Scene ID: LC08_L2SP_034032_20201006_20201016_02_T1. Available: USGS Explorer http://earthexplorer.usgs.gov. (October 15, 2020).

Vermote, E., Justice, C., Claverie, M., and Franch, B. (2016). "Preliminary analysis of the perforance of the Landsat 8/OLI land surface reflectance product." Remote Sensing of Environment, 185, 46–56., doi: 10.1016/j.rse.2016.04.008.

Wang, W.C., Dawdy, D.R. (2012). "Estimating Basin Storage Coefficient of the Clark Unit Hydrograph" American Geophysical Union Fall Meeting.

Woolridge, Douglas D., Niemann, Jeffrey D., Perry, Mark A., Bauer, Kallie E., McCormick III, William T. (2020). "Identifying Runoff Production Mechanisms for Dam Safety Applications in the Colorado Front Range." Journal of Hydrologic Engineering, vol. 25, no. 8, p. 05020016., doi:10.1061/(asce)he.1943-5584.0001958.

Yen, B. C., & Chow, V. T. (1983). Local design storms, Vol III. Rep. H 38 No. FHWA-RD-82/065, U.S. Dept. of Transportation, Federal Highway Administration, Washington, D.C. 1983.

Yoo, Chulsang, Lee, Jiho, Park, Changyeol, Jun, Changhyun. (2014). "Method for Estimating Concentration Time and Storage Coefficient of the Clark Model Using Rainfall-Runoff Measurements." Journal of Hydrologic Engineering, vol. 19, no. 3, pp. 626–634., doi:10.1061/(asce)he.1943-5584.0000828.

Young, C. Bryan, Nelson, Brian R., Bradley, A. Allen, Smith, James A., Peters-Lidard, Christa D., Kruger, Anton, Baeck, Mary Lynn. (1999). "An Evaluation of Nexrad Precipitation Estimates in Complex Terrain." Journal of Geophysical Research: Atmospheres, vol. 104, no. D16, pp. 19691–19703., doi:10.1029/1999jd900123.

Zecharias, Yemane B., and Wilfried Brutsaert. (1988). “Recession Characteristics of Groundwater Outflow and Base Flow from Mountainous Watersheds.” Water Resources Research, vol. 24, no. 10, pp. 1651–1658., doi:10.1029/wr024i010p01651.

Zhang, Yongqiang, and Francis H. Chiew. (2009). “Relative Merits of Different Methods for Runoff Predictions in Ungauged Catchments.” Water Resources Research, vol. 45, no. 7, doi:10.1029/2008wr007504.

Zhang, Z., Koren, V., Smith, M., Reed, S., and Wang, D. (2004). “Use of Next Generation Weather Radar Data and Basin Disaggregation to Improve Continuous Hydrograph Simulations.” Journal of Hydrologic Engineering, 9(2), 103–115., doi: 10.1061/(asce)1084-0699(2004)9:2(103).

Zier, James L., and William L. Baker. (2006). “A Century of Vegetation Change in the San Juan Mountains, COLORADO: An Analysis Using Repeat Photography.” Forest Ecology and Management, vol. 228, no. 1-3, pp. 251–262., doi:10.1016/j.foreco.2006.02.049.

Zoch, Richmond T. (1937). “On the Relation between Rainfall and Stream Flow—Iii.” Monthly Weather Review, vol. 65, no. 4, pp. 135–147., doi:10.1175/1520-0493(1937)65<135:otrbra>2.0.co;2.

APPENDIX A.
DETAILED INSTRUCTIONS FOR BASIN DELINEATION AND MODEL CREATION IN HEC-HMS

Instructions Demonstrating HEC-HMS GIS Capabilities

- Download DEM from National Elevation Dataset
  - File type should be .tif
    - https://viewer.nationalmap.gov/basic/

- Download stream gauge location and basin shapefile from USGS StreamStats
    - https://StreamStats.usgs.gov/ss/

  - The stream gauge will be labeled as globalwatershedpoint.shp

- Open HEC-HMS
  - Create a new project and navigate to where you want to save the model file
    - Select metric units
  - Create a basin model: Components >> Basin Model Manager
  - Create a terrain model: Components >> Terrain Model Manager
    - There will be an option to set a file path, click this and navigate to where the DEM is saved. Select the file shown (it will add a .tif extension)

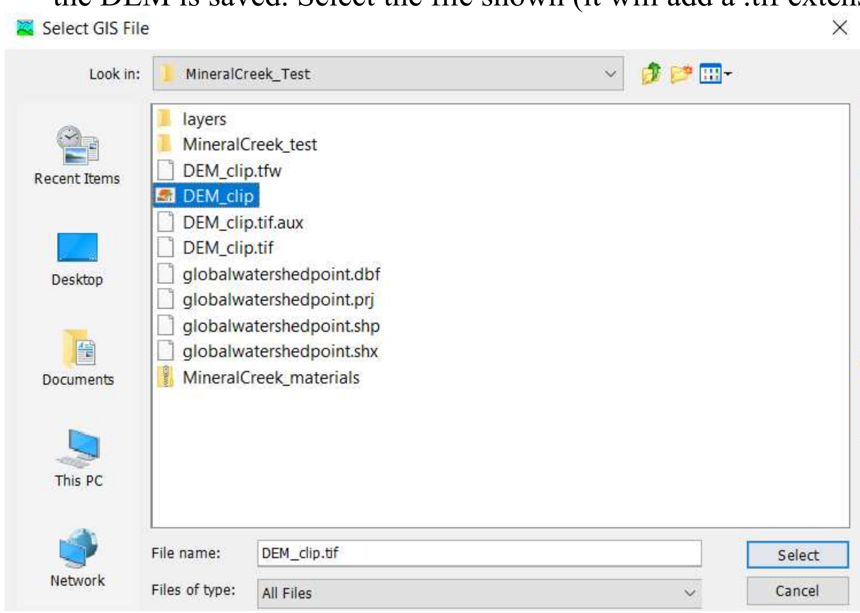

  - In the watershed explorer, click on the basin model
    - In the component editor, there will be a box that allows you to specify "Terrain Data". Select the terrain model you created above.
  - Go to the GIS menu, and choose coordinate system
    - Choose predefined
    - Select Universal Transverse Mercator (UTM) and then select zone 13N (this zone covers the majority of Colorado, only a small portion of the western part of the state falls in zone 12N). All of the proposed basins in this study will be in 13N.
    - Click select and then set

- If you click away from the basin model and back the terrain data should be visible.
- Under the GIS tab, select “Process Sinks” – HMS will then identify and fill in any drainage sinks in the DEM
- Under the GIS tab, select “Process Drainage” – this step combines the creation of a flow direction and flow accumulation grids.
- Under the GIS tab, select “Identify Streams” – this will create a raster of streams based on a specified area threshold. For our purposes, enter 15 km^2 as the threshold.
- [this step is optional] Right click anywhere in the basin model window and select “Map Layers”
    - Here you can see all the layer you have created thus far (DEM, Flow Direction, etc).
    - Click the “Add” option
        - Navigate to where you have saved the stream gauge location shapefile from StreamStats and add it to the map (the shapefile will automatically be updated in the specified coordinate system of all the other layers)
    - Once you have added the gauge location file, turn off all map layer except the gauge location and the Identified streams layers
    - Zoom into the gauge location point next to the stream raster. It is common for the gauge point to be located off the stream raster. That will be fixed in the next step.
- On the toolbar at the top of the program, there is an icon called “Break Point Creation Tool”. Click this icon. You may now specify any point on the stream raster to delineate a watershed from.

    - Click on a point on the stream that is closest to the stream gauge shapefile.
- Under the GIS tab, select “Delineate Elements”
    - A dialogue box will then appear
        - Set subbasin prefix to “Sub-“
        - Set reach prefix to “Reach-“
        - Select “Yes” for insert junctions
        - Set junction prefix to “Junction-“
        - Select “Yes” for convert breakpoints
    - Click OK and HMS will delineate your watershed and create a sub-basin and reach structure
- To export the sub-basin structure as a shapefile for use in ArcMap, select the “Export Georeferenced Elements” under the GIS tab. Navigate to the location you want to save the shapefile.

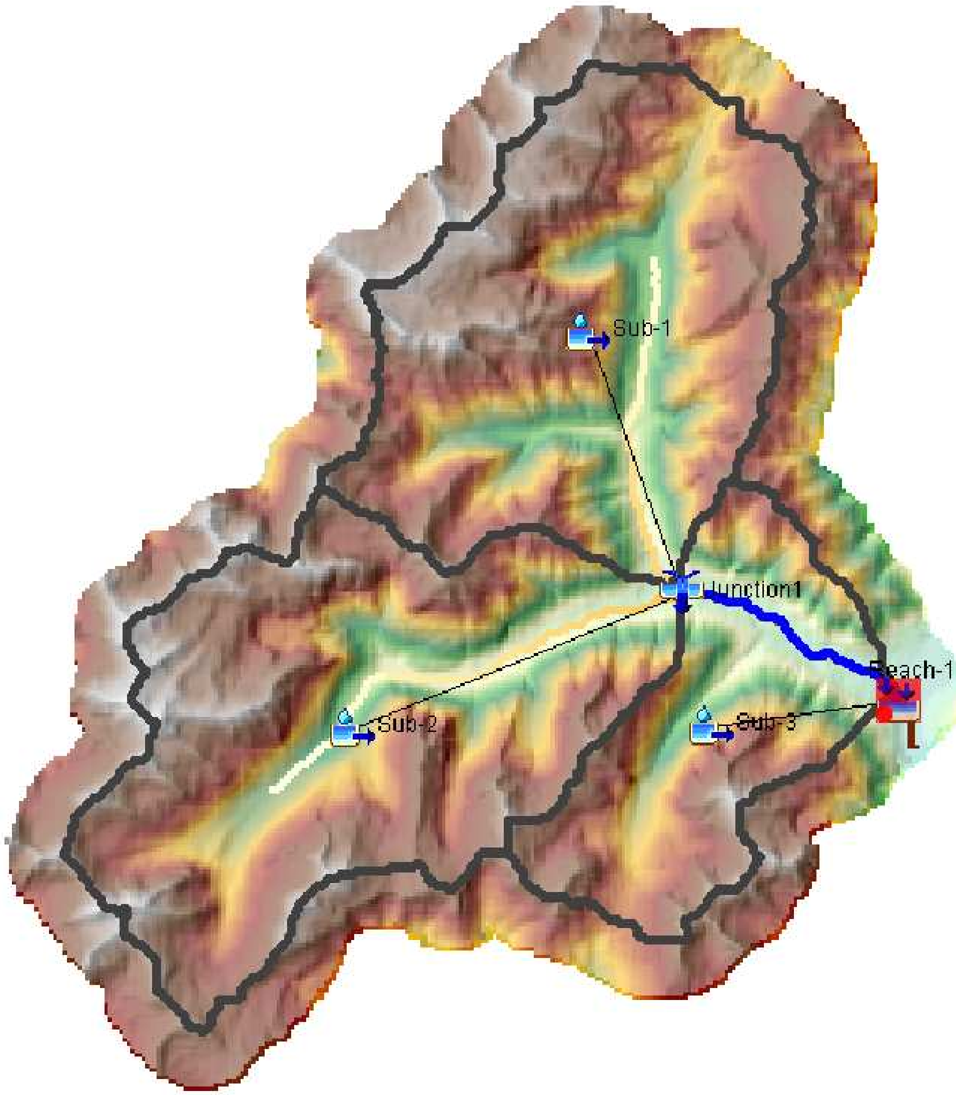
Sub-1
Junction1
Reach-1
Sub-2
Sub-3

APPENDIX B.

PYTHON CODE FOR DEVELOPING SOIL MOISTURE ACCOUNTING PARAMETERS

```
import numpy as np
import arcpy
import math
from arcpy.sa import *
from arcpy.conversion import *
arcpy.CheckOutExtension("Spatial")
arcpy.CheckOutExtension("3D")
arcpy.env.overwriteOutput = True

sand = "C:\\Users\\benirvin\\Desktop\\CO_gNATSGO\\SanJuan_SoilRasters\\p_sand"
clay = "C:\\Users\\benirvin\\Desktop\\CO_gNATSGO\\SanJuan_SoilRasters\\p_clay"
OM = "C:\\Users\\benirvin\\Desktop\\CO_gNATSGO\\SanJuan_SoilRasters\\p_om"
subs = "T:\\Projects\\jdngroup\\Ben_Research\\Model_Tests\\AWA_sub-
basins\\VallecitoCreek.shp"
aspect =
"T:\\Projects\\jdngroup\\Doug_Research\\GIS\\metric\\Elevation\\Bear\\bear_nf_sf_polys.shp"
d_restr =
"C:\\Users\\benirvin\\Desktop\\CO_gNATSGO\\Colorado_SoilRasters\\dtr_rclss"
Vc =
Raster("C:\\Users\\benirvin\\Desktop\\CO_gNATSGO\\SanJuan_SoilRasters\\f_veg")
asp_subs =
"T:\\Projects\\jdngroup\\Doug_Research\\GIS\\metric\\Basin_Delineations\\Bear\\20181206_Bea
r_Subs_asp.shp"


def Pedotransferfn(sand,aspect,clay,OM,sub,d_restr,Vc,asp_subs):

  ## set extent of sand, silt, clay, OM Rasters

  tempEnvironment0 = arcpy.env.extent
  tempEnvironment1 = arcpy.env.cellSize
  tempEnvironment2 = arcpy.env.snapRaster
  arcpy.env.extent = sub
  arcpy.env.cellSize = sub
  arcpy.env.snapRaster = sub
  sandsub = ExtractByMask(sand,sub)
  claysub = ExtractByMask(clay,sub)
  OMsub = ExtractByMask(OM,sub)

  # Convert % to fraction
  sandsub = sandsub / 100
  claysub = claysub / 100
  OMsub = OMsub / 100

  ## calculate theta_s with pedotransfer functions from Saxton and Rawls (2006); Eqs 2-
3, 5
```

```
	theta_33t = -0.251*sandsub + 0.195*claysub + 0.011*OMsub + 0.006*sandsub*OMsub
- 0.027*claysub*OMsub + 0.452*sandsub*claysub + 0.299
	theta_33 = theta_33t + 1.283*theta_33t**2 - 0.374*theta_33t - 0.015 # field capacity
soil moisture
	theta_s_33t = 0.278*sandsub + 0.034*claysub + 0.022*OMsub -
0.018*sandsub*OMsub - 0.027*claysub*OMsub - 0.584*sandsub*claysub + 0.078
	theta_s_33 = theta_s_33t + (0.636*theta_s_33t - 0.107)
	theta_s =
"C:\\Users\\benirvin\\Desktop\\CO_gNATSGO\\VallecitoCreek_Soils\\theta_s"
	if arcpy.Exists(theta_s):
	  arcpy.Delete_management(theta_s)
	theta_s = theta_33 + theta_s_33 - 0.097*sandsub + 0.043

theta_s.save("C:\\Users\\benirvin\\Desktop\\CO_gNATSGO\\VallecitoCreek_Soils\\theta_s")

theta_33.save("C:\\Users\\benirvin\\Desktop\\CO_gNATSGO\\VallecitoCreek_Soils\\theta_33")

	## calculate adjusted field capacity value for increased tension
	theta_fld_adj = theta_33 + 0.3*(theta_s - theta_33)

theta_fld_adj.save("C:\\Users\\benirvin\\Desktop\\CO_gNATSGO\\VallecitoCreek_Soils\\theta_
fld_adj")

	## calculate bare ground Ksat with pedotransfer functions from Saxton and Rawls
(2006); Eqs 15, 1, 18, 16
	B = "C:\\Users\\benirvin\\Desktop\\CO_gNATSGO\\VallecitoCreek_Soils\\B"
	theta_1500t = -0.024*sandsub + 0.487*claysub + 0.006*OMsub +
0.005*sandsub*OMsub - 0.013*claysub*OMsub + 0.068*sandsub*claysub + 0.031
	theta_1500 = theta_1500t + (0.14*theta_1500t-0.02) # wilting point soil moisture

theta_1500.save("C:\\Users\\benirvin\\Desktop\\CO_gNATSGO\\VallecitoCreek_Soils\\theta_15
00")
	B = 3.817/(Ln(theta_33) - Ln(theta_1500))
	lamda = 1/B
	Ksatbare =
"C:\\Users\\benirvin\\Desktop\\CO_gNATSGO\\VallecitoCreek_Soils\\Ksatbare"
	if arcpy.Exists(Ksatbare):
	  arcpy.Delete_management(Ksatbare)
	Ksatbare = 1930*(theta_s - theta_33)**(3 - lamda)

Ksatbare.save("C:\\Users\\benirvin\\Desktop\\CO_gNATSGO\\VallecitoCreek_Soils\\Ksatbare")
	B.save("C:\\Users\\benirvin\\Desktop\\CO_gNATSGO\\VallecitoCreek_Soils\\B")

lamda.save("C:\\Users\\benirvin\\Desktop\\CO_gNATSGO\\VallecitoCreek_Soils\\lamda")
```

```
## calculate psi_f using Saxton and Rawls, 2006 (Eqs 14, 4) and Rawls et al, 1983 (Eq. 4)
A = Exp(3.497 + B*Ln(theta_33))
psif = "C:\\Users\\benirvin\\Desktop\\CO_gNATSGO\\VallecitoCreek_Soils\\psif"
if arcpy.Exists(psif):
  arcpy.Delete_management(psif)
psiet = -21.67*sandsub - 27.93*claysub - 81.97*theta_s_33 + 71.12*(sandsub*theta_s_33) + 8.29*claysub*theta_s_33 + 14.05*sandsub*claysub + 27.16
psie = psiet + (0.02*psiet**2-0.113*psiet-0.7) # bubbling pressure in kPa from Saxton and Rawls, 2006
psie_head = psie / 9.81 * 1000 # kPa = 1000 N/m2 = 1000 (kg*m/s2) / m2 => head = P / rho*g => h = [1000 (kg * m/s2) / m2] / [(1000 kg/m3)(9.81 m/s2)]; in meters, then multiply by 1000 to convert to mm

psif = (2*lamda+3)/(2*lamda+2)*(psie_head/2) # wetting front section head in mm; Eq 4 from Rawls et al, 1983
psif.save("C:\\Users\\benirvin\\Desktop\\CO_gNATSGO\\VallecitoCreek_Soils\\psif")

## adjust bare ground ksat based on vegetation using Figure 8 in Sabol, 2008
ck = (Vc*100-10)/90 + 1
Ksat = Ksatbare*ck
Ksathalf = Ksat/2
Ksat.save("C:\\Users\\benirvin\\Desktop\\CO_gNATSGO\\VallecitoCreek_Soils\\Ksat")

Ksathalf.save("C:\\Users\\benirvin\\Desktop\\CO_gNATSGO\\VallecitoCreek_Soils\\Ksathalf")
ck.save("C:\\Users\\benirvin\\Desktop\\CO_gNATSGO\\VallecitoCreek_Soils\\ck")

## calculate maximum infiltration capacity based on Green-Ampt at representative depth
delta = 76.2 # representative depth of 3 inches in mm
f = "C:\\Users\\benirvin\\Desktop\\CO_gNATSGO\\VallecitoCreek_Soils\\maxinfil"
if arcpy.Exists(f):
  arcpy.Delete_management(f)
f = Ksat * (1 + psif/delta)
f_halfks = Ksathalf * (1 + psif/delta)
f.save("C:\\Users\\benirvin\\Desktop\\CO_gNATSGO\\VallecitoCreek_Soils\\maxinfil")

f_halfks.save("C:\\Users\\benirvin\\Desktop\\CO_gNATSGO\\VallecitoCreek_Soils\\f_halfks")


## calculate statistics of all soil properties by subbasin
arcpy.env.workspace = "C:\\Users\\benirvin\\Desktop\\CO_gNATSGO\\VallecitoCreek_Soils\\Output_Tables"
 d_restr = ZonalStatisticsAsTable(subs,"name", d_restr," d_restr _table_WA")
 f_table = ZonalStatisticsAsTable(subs,"name",f,"f_table")
f_halfks_table = ZonalStatisticsAsTable(subs,"name",f_halfks,"f_halfks_table")
```

```
    psif_table = ZonalStatisticsAsTable(subs,"name",psif,"psif_table")
    Ksat_table = ZonalStatisticsAsTable(subs,"name",Ksat,"Ksat_table")
    Ksathalf_table = ZonalStatisticsAsTable(subs,"name",Ksathalf,"Ksathalf_table")
    Ksatbare_table = ZonalStatisticsAsTable(subs,"name",Ksatbare,"Ksatbare_table")
    theta_s_table = ZonalStatisticsAsTable(subs,"name",theta_s,"theta_s_table")
    theta_33_table = ZonalStatisticsAsTable(subs,"name",theta_33,"theta_fld")
    theta_fld_adj_table =
ZonalStatisticsAsTable(subs,"name",theta_fld_adj,"theta_fld_adj")
    theta_1500_table = ZonalStatisticsAsTable(subs,"name",theta_1500,"theta_wp")

    arcpy.env.extent = tempEnvironment0
    arcpy.env.cellSize = tempEnvironment1
    arcpy.env.snapRaster = tempEnvironment2

    return f, Ksat, theta_s, psif

f,Ksat,theta_s,psi = Pedotransferfn(sand, aspect, clay, OM,subs,d_restr,Vc,asp_subs)
```

APPENDIX C.
SUPPLEMENTAL TABLES AND FIGURES

Table 5. Typical parameter values for Front Range and San Juan Range basins.

Basin	Max soil storage (mm)	Tension Storage (mm)	Groundwater Storage (mm)	Soil Percolation Rate (mm/h)	Max Infiltration Rate (mm/h)	Groundwater Percolation Rate (mm/h)
North Fork Big Thompson River	171.47	84.37	19.05	23.03	47.25	2.50
Big Thompson River	162.73	80.84	18.08	21.93	40.21	2.50
South Boulder Creek	153.16	74.40	17.02	24.77	54.33	2.50
Bear Creek	161.57	84.07	17.95	24.41	54.82	2.50
Cheyenne Creek	118.39	53.08	13.15	46.82	54.34	2.50
Vallecito Creek	142.15	83.76	7.48	8.01	33.69	0.50
Saguache Creek	148.54	73.25	7.43	8.85	25.85	0.50
Mineral Creek	157.02	97.50	8.26	6.92	30.09	0.50

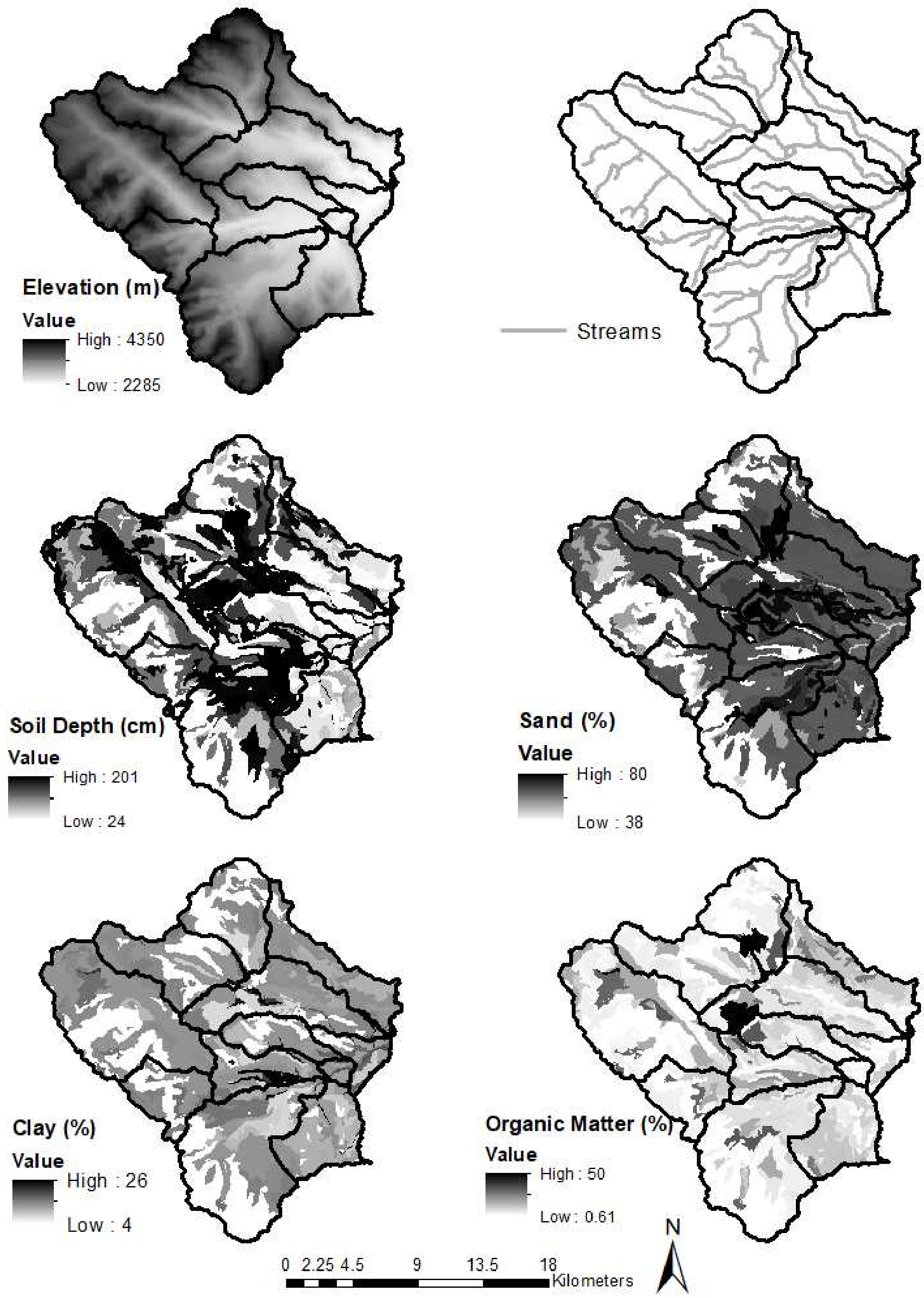

Figure 14. Required input data for model creation and parameter estimation for the Big Thompson River basin.

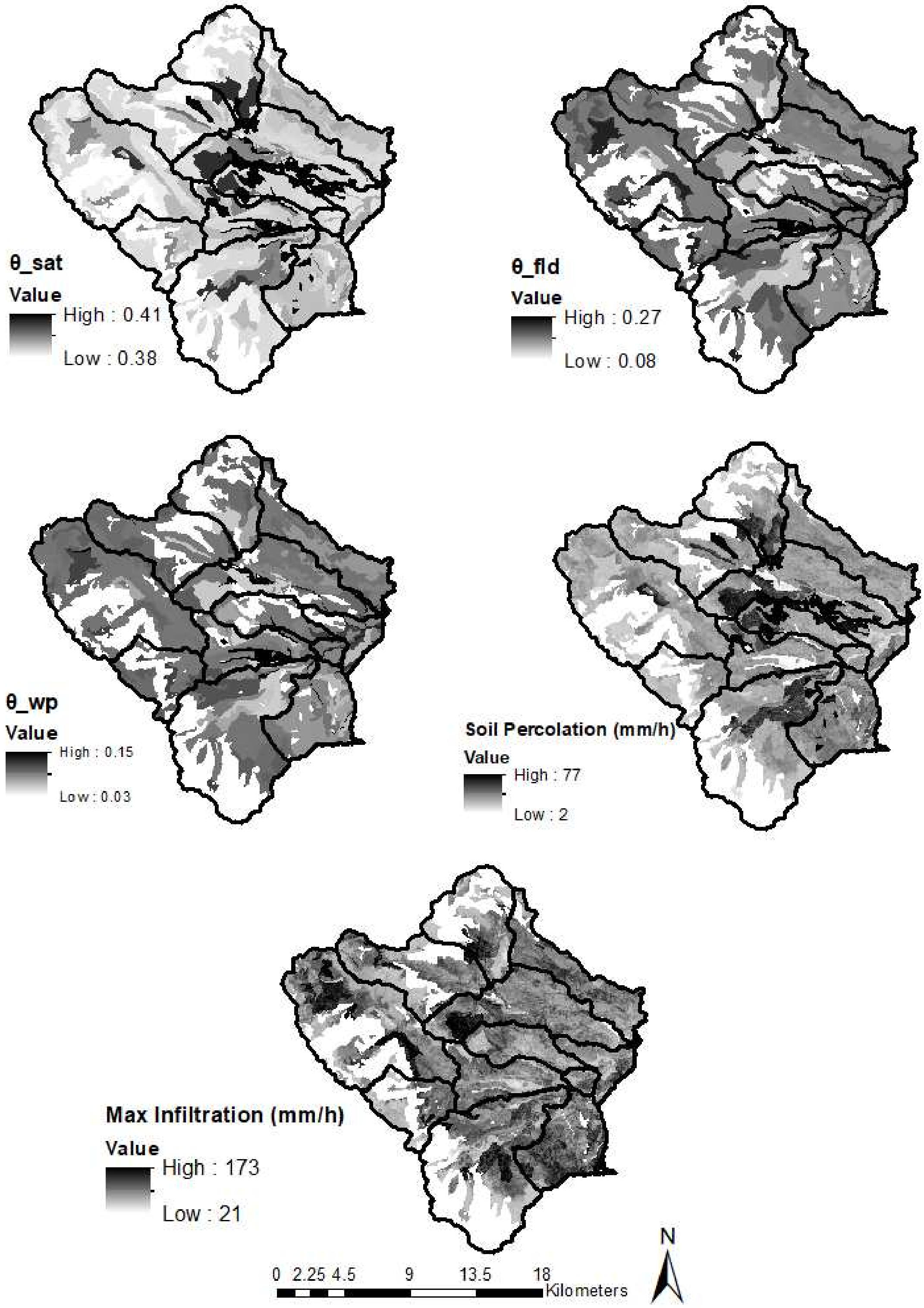

Figure 15. Soil hydraulic characteristics and parameters calculated for the Big Thompson River basin.